Use of ab Initio Calculations To Predict the Biological Potency of Carboxylesterase Inhibitors

Craig E. Wheelock,[†] Michael E. Colvin,[‡] Ippei Uemura,[§] Marilyn M. Olmstead,[||] James R. Sanborn,[†] Yoshiaki Nakagawa,[§] A. Daniel Jones,[⊥] and Bruce D. Hammock*,[†]

Department of Entomology and Cancer Research Center, University of California, Davis, California 95616, Biology and Biotechnology Research Program, Mailstop L-448, Lawrence Livermore National Laboratory, Livermore, California 94550, Division of Applied Life Sciences, Graduate School of Agriculture, Kyoto University, Kyoto 606-8502, Japan, Department of Chemistry, University of California, Davis, California 95616, and Department of Chemistry, The Pennsylvania State University, University Park, Pennsylvania 16802

Carboxylesterases are important enzymes responsible for the hydrolysis and metabolism of numerous pharmaceuticals and xenobiotics. These enzymes are potently inhibited by trifluoromethyl ketone containing (TFK) inhibitors. We demonstrated that the ketone hydration state was affected by the surrounding chemical moieties and was related to inhibitor potency, with inhibitors that favored the *gem*-diol conformation exhibiting greater potency. Ab initio calculations were performed to determine the energy of hydration of the ketone, and the values were correlated with esterase inhibition data for a series of carboxylesterase inhibitors. This system was examined in three different mammalian models (human liver microsomes, murine liver microsomes, and commercial porcine liver esterase) and in an insect enzyme preparation (juvenile hormone esterase). In all cases, the extent of ketone hydration was strongly correlated with biological potency. Our results showed a very strong correlation with the extent of hydration, accounting for 94% of activity for human liver microsome esterase inhibition ($p < 0.01$). The atomic charge on the carbon atom of the carbonyl group in the TFK also strongly correlated with inhibitor potency, accounting for 94% of inhibition activity in human liver microsomes ($p < 0.01$). In addition, we provide crystallographic evidence of intramolecular hydrogen bonding in sulfur-containing inhibitors and relate these data to *gem*-diol formation. This study provides insight into the mechanism of carboxylesterase inhibition and raises the possibility that inhibitors that too strongly favor the *gem*-diol configuration have decreased potency due to low rate of ketone formation.

Introduction

Carboxylesterases (EC 3.1.1.1) are a group of enzymes in the α/β hydrolase family that are important in the hydrolysis and subsequent metabolism of numerous therapeutic agents and xenobiotics.[1,2] They have extremely broad substrate selectivity, which makes their nomenclature somewhat confusing, and they are often collectively referred to as "esterases".[3] Carboxylesterases are of clinical importance because of their high abundance, ability to hydrolyze numerous pharmaceuticals, and location in a diverse array of tissues, including liver, blood plasma, lung, small intestine, brain, stomach, spleen, heart, testis, prostate, pancreas, colon, macrophages, and monocytes (refs 2 and 4 and references therein). They hydrolyze a wide array of drugs and xenobiotics, including the β-blockers flestolol[5] and esmolol,[6] the Ca^{2+}-activated K^+ channel blocker cetiedil,[7] cocaine, and heroin[4,8] and are important in the transesterification of meperidine (Demerol) and methylphenidate (Ritalin).[9] The hydrolytic activity of carboxyl-

esterases has been employed to design prodrugs such as the anti-HIV drug glycovir,[10] L-DOPA ester anti-Parkinsonian agents,[11] the blood cholesterol drug lovastatin,[12] and the chemotherapeutic agent CPT-11.[13−16] Carboxylesterase activity has also been used to reduce the gastrotoxicity of ibuprofen by masking the free carboxylic acid with an ester group that is hydrolyzed in vivo.[17] Carboxylesterases may play a role in protecting the male reproductive system against xenobiotics[18,19] and have been demonstrated to inhibit invasion of the malaria sporozite *Plasmodium falciparum* in human hepatocytes.[20] In addition, carboxylesterases are key enzymes in the metabolism and detoxification of pyrethroid,[21] organophosphate,[22] and carbamate[23] insecticides.

The pharmacokinetic behavior of ester-containing compounds is highly influenced by esterlytic activity, with many prodrugs and soft drugs relying on carboxylesterase activity for activation and deactivation, respectively.[3,24,25] One difficulty encountered in the activation of these compounds is effecting the controlled release of active agent over time, since this is dependent on endogenous enzyme activity. For example, flestolol has a half-life of ∼5−10 min in human plasma and its primary route of metabolism is via esterases. It is estimated that only 5% of the active drug reaches the target site.[26] From a therapeutic standpoint, it could be

* To whom correspondence should be addressed. Phone: 530-752-7519. Fax: 530-752-1537. E-mail: bdhammock@ucdavis.edu.
† Department of Entomology and Cancer Research Center, University of California, Davis.
‡ Lawrence Livermore National Laboratory.
§ Kyoto University.
|| Department of Chemistry, University of California, Davis.
⊥ The Pennsylvania State University.
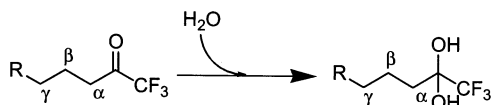
Figure 1. Hydration reaction of trifluoromethyl ketone from the ketone to the *gem*-diol. Greek letters indicate carbon positions relative to the carbonyl (*gem*-diol) referred to in the text.

useful to have selective enzyme inhibitors to regulate enzyme activity and subsequent prodrug activation and drug residence time. Alternatively, unanticipated esterase inhibition could dramatically alter the potency of pharmaceuticals. In addition, inhibiting a metabolic pathway can be an effective method to study the metabolism and fate of a compound.

The most potent inhibitors of carboxylesterases found to date are a group of compounds collectively known as trifluoromethyl ketones (TFKs), consisting of a trifluoromethyl group placed α to a ketone (Figure 1).[27] The trifluoroacyl chemical moiety is very efficient at inhibiting enzymes whose catalytic mechanisms involve a nucleophilic attack by a catalytic residue in the enzyme active site.[28] There are several examples of important enzymes that have been successfully inhibited by compounds containing this moiety including acetylcholinesterase,[29] HIV-1 protease,[30] human leukocyte[31] and neutrophil elastase,[32] fatty acid amide hydrolase,[33] and carboxylesterase.[34] The extreme potency of these compounds is due to the polarization of the carbonyl by the trifluoromethyl group, thereby greatly increasing the electrophilicity of the carbonyl carbon and subsequently increasing its susceptibility to nucleophilic attack.[35] The potency of TFK-containing compounds has also been attributed to their being transition state analogue (TSA) inhibitors.[36] Upon binding to the enzyme, these inhibitors form a tetrahedral complex that mimics the transition state of the enzyme–substrate complex.[37,38] Since there is no cleavable chemical bond, the enzyme is inhibited. The large number of TFK-containing carboxylesterase inhibitors reported in the literature have been extensively analyzed via quantitative structure–activity relationship (QSAR) techniques.[35,39] The resulting equations contained multiple parameters to accurately describe the biological potency of these compounds. The majority of the developed equations relied on molar refractivity or lipophilicity as the major descriptors and did not examine electronic effects in detail. However, it has also been shown that increasing the degree of fluorination generally increases inhibitor potency.[35]

Brodbeck et al.[40] reported the first use of the TFK moiety in enzyme inhibition for acetylcholinesterase in 1979, and Hammock and co-workers showed in 1982 that TFK-containing inhibitors were potent on other carboxylesterases.[36] Successive modifications of this structure involved substituting a sulfur atom β to the carbonyl[36,41] and various degrees of unsaturation at the α position[42] as well as alkyl substitutions α and γ to the carbonyl[43] (Figure 1). These alterations had a large effect on inhibitor strength, with the sulfur-containing inhibitors exhibiting the greatest potency. However, the mechanism for the increased potency of the sulfur compounds was not well understood. There have been several hypotheses set forth,[34,35,44] but none has ad-

equately accounted for inhibitor activity. We therefore designed this study to further refine the structure–activity relationship of the TFK-containing carboxylesterase inhibitors.

In TFK-containing inhibitors, the polarization of the carbonyl shifts the equilibrium toward the *gem*-diol form (Figure 1).[44] Linderman et al. demonstrated that ab initio calculations could be used to estimate the electrophilicity of the carbonyl of the TFK moiety, which was demonstrated to be correlated with biological activity.[45,46] We hypothesized that the activity of carboxylesterase inhibitors might be predicted based on their degree of ketone hydration. Inhibitors that electronically favor the tetrahedral sp³-hybridized geometry of the hydrated state (*gem*-diol), versus the trigonal planar sp²-hybridized carbonyl, should also favor this conformation in the inhibited enzyme. Therefore, moieties that support the tetrahedral geometry should stabilize the enzyme-bound inhibitor complex, thus increasing the strength of the inhibitor bond and resulting in a more potent inhibitor. To quantitatively examine this effect, it was necessary to determine the ketone/*gem*-diol equilibrium for a series of inhibitors with varying substituents surrounding the ketone moiety. Another theory for the activity of TFK inhibitors predicts that a hydroxy group in the *gem*-diol forms an intramolecular hydrogen bond with groups in the β position (Figure 1). It is hypothesized that this bond stabilizes both the *gem*-diol form of the inhibitor and the enzyme-bound inhibitor complex, leading to increased inhibitor potency. To test this hypothesis, we estimated the potential for formation of the intramolecular hydrogen bonds and determined if the bond strengths correlated with inhibitor potency.

We predicted the degree of hydration of inhibitors by calculating the electronic energy (ΔE) and the Gibb's free energy (ΔG, given by $\Delta G = \Delta H - T\Delta S$) for the ketone/*gem*-diol equilibrium reaction. The magnitude and sign of the energy term determines the relative concentration of ketone/*gem*-diol at equilibrium. It would be difficult to accurately measure the ketone/*gem*-diol equilibrium, and the result would depend on the physical environment in which the experiments were performed (i.e., gas, aqueous, or protein microenvironment). We therefore used ab initio quantum chemical calculations to determine the energies of ketone hydration to form the *gem*-diol. These calculations were performed in both gas phase (dielectric constant $\epsilon = 1$) and aqueous phase environments ($\epsilon = 78.34$) to determine the effects of the physical environment on the equilibrium state. We correlated these modeling data with the biological potency of the inhibitors to determine the relationship between inhibitor potency and degree of ketone hydration. We were then able to synthesize inhibitors of varying inhibition potency based on hydration energy calculations. The results of this study allowed us to accurately predict inhibitor potency before undertaking time-consuming syntheses and enabled us to further evaluate the use of ab initio calculations as a tool to predict biological activity. In addition, results of this study have provided evidence explaining the mechanism of the increased potency of sulfur-containing carboxylesterase inhibitors.

Overview of Computational Chemical Methods

A wide variety of chemical simulation methods have been developed, ranging from empirical ball-and-spring type molecular mechanics models to ab initio (first principles) quantum chemical methods that calculate approximate solutions to the exact quantum mechanical equations describing the electrons and nuclei. Typically, the choice of methods involves tradeoffs among accuracy, size of the chemical system, and computational cost. There is a hierarchy of different quantum chemical methods involving increasingly accurate mathematical descriptions of the electronic wave function, the mathematical description of the distribution of electrons around the nuclei of a molecule.[47] Over the past 2 decades, a class of methods called density functional theory (DFT) has been developed that includes empirical parametrizations of the electron–electron interactions and often provides accuracy comparable to that of the earlier high-level quantum chemical methods but with a much lower computational cost. The DFT methods are usually denoted by the empirical electron–electron "functional" employed. Two widely used DFT functionals are the Becke three-parameter hybrid exchange functional (B3) and the Lee–Yang–Parr (LYP) gradient-corrected electron correlation functional[49] that have been widely demonstrated to yield accurate chemical structures and reaction energies when used with sufficient basis sets for most molecules.[47]

An important limitation of the quantum chemical methods described above is that they describe only an isolated (usually described as "gas-phase") molecule and therefore do not include the chemical environment, such as solvent molecules and counterions. Explicitly including the surrounding molecules is usually too computationally costly for quantum chemistry methods; however, several methods have been developed within the quantum chemistry approach for including the effects of solvent interactions. Typically these methods model the solvent as a continuous medium that polarizes in response to the quantum chemically derived charges. Although there are situations where explicit inclusion of the solvent is necessary, these so-called polarizable continuum models (PCM) have proven to be reasonably accurate in predicting solvent-phase chemical properties including total solvation energies and acid constants.[50,51] One version of PCM, the conductor-like screening solvation model COSMO,[52] models the surrounding solvent by means of polarization charges distributed on the solvent-exposed surface of the molecule. Although structural optimizations can be performed using these PCM solvent models, earlier studies have shown that for most molecules reoptimizing in the solvent does not significantly affect the solution-phase energies.[51]

A method related to these polarizable continuum models but including a more realistic representation of the polar solvent is the Langevin dipole method of Warshel (ChemSol),[53] which models the solvent as a large set of polarizable dipoles on a fixed three-dimensional grid.[54] This approach has recently been parametrized for use with ab initio derived solute charges and shown to yield solvation energies for neutral and ionic molecules comparable to or better than PCM methods and has been extensively applied to the problem of phosphate hydrolysis.[53] Where the appropri-ate parameters were available (the ChemSol method does not have the appropriate parameters for the selenium atom), we also used the Langevin dipole method to calculate the effects of aqueous solvation on the hydration reaction energies of the compounds.

In addition to molecular structures and energies, another frequently calculated value from the electronic wave function is the effective atomic charges, the net electronic and nuclear charge on each atom. Historically, Mulliken population analysis has been widely used, but the derived atomic charges have proved to be extremely sensitive to the molecular configuration and wave function. Another method, natural atomic population analysis (NPA), has been developed that overcomes most of the limitations of the earlier method[55] and yields atomic charges that validate many qualitative chemical concepts.

Methods

We were particularly interested in the role of the sulfur atom in inhibitor potency because several researchers have reported the ability of this atom to confer enhanced inhibition potency for esterase inhibition.[34–36,44] We therefore weighted our selection of compound structures for study toward sulfur-containing inhibitors (Tables 1 and 2). The energy of hydration calculations were performed in a number of different environments in order to determine the optimal parameters for the correlation (Tables 3 and 4). A total of five different energies were examined: the electronic energy in the gas phase (ΔE_{gas}), the energy in the aqueous phase (ΔE_{aq}), the free energy in the gas phase (ΔG_{gas}), and the free energy in the aqueous phase using two different calculation methods, the PCM model (ΔG_{aq}, COSMO) and the Langevin dipole model (ΔG_{aq}, ChemSol). The significance of the correlation values was then compared for all enzymes for each energy value. These terms are further defined in the Supporting Information.

Quantum Chemical Calculations. The molecular structures of the ketone and hydrated (*gem*-diol) forms of each inhibitor were built using AMPAC.[56] The alkane chains were built in the fully extended all-trans conformation, consistent with recent experimental data for aqueous phase saturated alkanes.[57] All structures were optimized using DFT with the B3LYP functional using a 6-31G* basis set. The free energies (298 K) of these structures were determined from the total B3LYP/6-31G* electronic energies of the optimized molecular structures combined with vibrational, thermal, and entropic terms calculated from the B3LYP/6-31G* harmonic vibrational frequencies using standard formulas.[58] The atomic charges were predicted using NPA from the B3LYP/6-31G* wave function at the B3LYP/6-31G* optimized geometries. Aqueous phase solvation free energies were calculated using either the COSMO or ChemSol solvation model coupled to the B3LYP/6-31G* wave function at the gas phase optimized geometries, based on previous theoretical studies showing that reoptimizing the gas phase structures within the PCM solvent models has very little effect on the results.[51]

All quantum chemical calculations were performed using Guassian 98, revision A.7.[59] The Langevin dipole calculations were performed using ChemSol version

Table 1. Structure and Calculated log *P* Data for Synthesized Compounds

no.	Compound[a]	ClogP[b] Ketone	ClogP[b] *Gem*-diol[c]
1		3.49	2.95
2		3.79	2.67
3		4.05	3.71
4		3.72	3.62
5		3.00	4.15
6		3.46[d]	2.90
7		1.87	1.17
8		2.90[e]	2.14
9		1.31	0.41
10		2.76	2.14
11		2.20	1.38
12		1.95	1.26
13		2.25	0.50

[a] All compounds have a hexyl ($CH_3(CH_2)_5$) moiety as the R group. [b] Calculated log *P* (ClogP) values were determined using the ClogP program of Leo.[64] [c] ClogP determinations were also performed for the hydrated ketone (*gem*-diol). [d] The measured log *P* value was 3.09 ± 0.02 (*n* = 3). [e] The measured log *P* value was 3.83 ± 0.04 (*n* = 3).

2.1.[60] All calculations were run on Compaq AlphaServer 4100 model 5/533 quadprocessor workstations with a 533 MHz EV5.6 CPU running OSF, version 5.1.

Hydrogen Bond Strength Calculations. The intramolecular hydrogen bond strengths for the thioether and sulfone containing compounds were estimated using calculations on model *gem*-diol compounds (see Results and Discussion). These compounds were fully optimized as described above, and single-point solution-phase calculations where calculated using the COSMO or ChemSol models with dielectric constants that mimic three different solvents: water ($\epsilon = 78.39$), methanol ($\epsilon = 32.63$), and benzene ($\epsilon = 2.247$). These structures were then reoptimized with inclusion of internal constraints on the rotations of the *gem*-diol hydroxyl groups to prohibit hydrogen bonding to the thioether sulfur atom or the sulfone oxygen atoms. The intramolecular hydrogen bond energies were then estimated as the difference in electronic energies between the constrained and unconstrained structures.

Table 2. Structure and Calculated log *P* Data for Theoretical Compounds

no.	Compound[a]	ClogP[b] Ketone	ClogP[b] *Gem*-diol[c]
14		3.31	2.74
15		2.81	2.19
16		2.81	2.19
17		2.75	1.99
18		2.25	1.43
19		2.25	1.43
20		2.53	1.89
21		4.35	2.99
22		3.79	2.67

[a] All compounds have a hexyl ($CH_3(CH_2)_5$) moiety as the R group. [b] Calculated log *P* (ClogP) values were determined using the ClogP program of Leo.[64] [c] ClogP determinations were also performed for the hydrated ketone (*gem*-diol).

Table 3. Calculated Hydration Energies for Synthesized Compounds

no.	ΔE_{gas} [a]	ΔG_{gas} [b]	ΔE_{aq} [c]	ΔG_{aq} (COSMO) [d]	ΔG_{aq} (ChemSol) [e]	carbonyl charge[f]
1	−4.72	10.01	−5.05	9.69	15.0	0.594
2	−12.99	1.58	−12.17	2.40	6.3	0.523
3	−13.15	2.00	−12.65	2.51	7.7	0.499
4	−7.17	7.50	−6.67	8.01	14.5	0.444
5	−9.16	3.81	−10.14	2.82	9.5	0.416
6	−19.51	−2.60	−16.74	0.17	4.2	0.484
7	−17.42	−2.23	−14.98	0.21	2.9	0.479
8	−12.30	3.78	−9.58	6.50	12.3	0.582
9	−8.73	5.95	−5.69	8.99	12.2	0.573
10	−19.77	−4.46	−17.80	−2.49	0.4	0.482
11	−11.11	4.69	−8.75	7.05	11.2	0.576
12	−25.06	−10.25	−21.69	−6.88	−0.4	0.467
13	−15.05	1.38	−11.06	5.37	10.9	0.567

[a] Energy of hydration in the gas phase (kcal/mol). [b] Free energy of hydration in the gas phase (kcal/mol). [c] Energy of hydration in the aqueous phase using the COSMO solvation model (kcal/mol).[52] [d] Free energy of hydration in the aqueous phase using COSMO solvation model (kcal/mol).[52] [e] Free energy of hydration in the aqueous phase using the Langevin dipole (ChemSol) solvation model (kcal/mol).[53] [f] Calculated atomic charge on the carbonyl carbon (eV).

Results and Discussion

Trifluoromethyl ketones are potent inhibitors of carboxylesterases. However, modulation of inhibitor potency may be desirable for different goals. Ab initio calculations were performed to test the hypothesis that the hydration state of the inhibitory ketone function is a critical component of carboxylesterase inhibition. An initial model was developed with juvenile hormone esterase (JHE) from the cabbage looper *Trichoplusia ni* and then applied to three mammalian systems. This enzyme was chosen to develop the correlative model

Table 4. Calculated Hydration Energies for Theoretical Compounds

no.	ΔE_{gas} [a]	ΔG_{gas} [b]	ΔE_{aq} [c]	ΔG_{aq} (COSMO)[d]	ΔG_{aq} (ChemSol)[e]	carbonyl charge[f]
14	−17.35	−2.16	−15.05	0.14	g	0.449
15	−24.40	−9.47	−21.55	−6.61	g	0.449
16	−21.12	−5.71	−17.61	−2.20	g	0.465
17	−11.06	4.04	−8.88	6.22	g	0.561
18	−14.01	1.27	−10.31	4.97	g	0.558
19	−12.05	3.10	−9.48	5.67	g	0.573
20	−20.60	−5.42	−16.62	−1.45	−1.0	0.491
21	−18.61	−3.53	−19.29	−4.21	0.4	0.442
22	−9.29	5.47	−6.94	7.82	12.6	0.556

[a] Energy of hydration in the gas phase (kcal/mol). [b] Free energy of hydration in the gas phase (kcal/mol). [c] Energy of hydration in the aqueous phase using the COSMO solvation model (kcal/mol).[52] [d] Free energy of hydration in the aqueous phase using COSMO solvation model (kcal/mol).[52] [e] Free energy of hydration in the aqueous phase using the Langevin dipole (ChemSol) solvation model (kcal/mol).[53] [f] Calculated atomic charge on the carbonyl carbon (eV). g The value was not determined because the ChemSol method lacks parameters for the selenium atom.

given that a single predominant isozyme in *T. ni* hemolymph is responsible for the hydrolysis of juvenile hormone,[61,62] thus reducing the potential for the effects of multiple isozymes with different inhibition profiles. Additionally, there is a large body of data available for JHE inhibition by TFK-containing compounds.[34,41,42,63]

This study was initiated by mining data for a series of six compounds (**1**−**6**) from the available JHE literature.[35,36] The initial results showed a positive correlation between the hydration state of the ketone and inhibitor potency (data not shown). Compounds were then designed to explore the effects of potential functional groups surrounding the ketone moiety (Tables 1 and 2, compounds **7**−**22**). We used our initial regression equations for JHE to predict the biological potency of these new compounds in an attempt to predict the most potent inhibitors.

There have been a number of published studies on the potency of TFK inhibitors[35,39,42,43] that have identified lipophilicity as a key parameter in determining inhibitor potency. For many esterases, the most potent inhibitors have large log P values (>3). Therefore, to reduce the hydrophobic variance, the inhibitor alkyl chain was fixed at six carbons. In addition, the calculated energies of hydration were evaluated for covariance with lipophilicity. The log P values for both the ketone and *gem*-diol forms of the inhibitors were determined using Leo's ClogP program (Tables 1 and 2).[64] To test the ability of this program to estimate partition coefficients for these compounds, we measured log P values for compounds **6** and **8**. Work by Thomas et al. reported that it was not possible to directly measure octanol/water partitioning for these hydrated ketone compounds because of hemiacetal formation.[65] The partition coefficient was therefore determined in cyclohexane and calculated for octanol using a solvent regression equation. Results indicated that predicted values were within 1 order of magnitude of measured values (Table 1). This observed trend was in close agreement with that of Thomas and co-workers.[65] It is important to remember that any equilibrium measured represents both compound partitioning and possible shifts in hydration, thereby affecting the final value. Additionally, even the "experimental" log P had to be

Table 5. Inhibition of Carboxylesterase Activity by Synthesized Compounds[a]

no.	human −log IC_{50}	murine −log IC_{50}	porcine −log IC_{50}	JHE[b] −log IC_{50}
1	2.07[c]	0.77[c]	1.17[c]	2.15[d]
2	5.30[c]	4.35[c]	4.61[c]	5.00[d]
3	5.36[c]	4.42[c]	4.67[c]	5.17[d]
4	3.03[c]	1.83[c]	2.19[c]	4.10[e]
5	3.80[c]	2.69[c]	3.02[c]	6.40[e]
6	8.16 ± 0.03	7.90 ± 0.04	8.08 ± 0.02	7.51 ± 0.01
7	7.33 ± 0.01	6.35 ± 0.01	6.17 ± 0.01	6.83 ± 0.02
8	4.55 ± 0.09	3.02 ± 0.12	3.01 ± 0.09	2.86 ± 0.07
9	3.98 ± 0.03	3.32 ± 0.04	3.96 ± 0.06	3.29 ± 0.04
10	7.32 ± 0.01	6.92 ± 0.06	7.36 ± 0.08	7.08 ± 0.01
11	4.26 ± 0.03	3.37 ± 0.05	3.59 ± 0.02	3.31 ± 0.12
12	6.51 ± 0.02	6.35 ± 0.01	6.77 ± 0.03	5.85 ± 0.03

[a] IC_{50} is the concentration of inhibitor at which 50% of enzyme activity was inhibited. Data for compound **13** are excluded because of instability. [b] Juvenile hormone esterase (JHE) from the cabbage looper *Trichoplusia ni*. [c] Data estimated from linear regression for each enzyme using ΔE_{gas} regression values (see Table 7). [d] Data from Hammock et al.[36] [e] Data from Székács et al.[35]

Table 6. Predicted Inhibition of Carboxylesterase Activity by Theoretical Compounds[a]

no.	human[b] −log IC_{50}	murine[b] −log IC_{50}	porcine[b] −log IC_{50}	JHE[b,c] −log IC_{50}
12[d]	10.00	9.59	9.62	9.39
13[d]	6.10	5.25	5.46	4.29
14	7.00	6.24	6.42	6.46
15	9.75	9.30	9.34	9.27
16	8.47	7.88	7.98	7.44
17	4.54	3.52	3.81	3.93
18	5.69	4.80	5.03	4.45
19	4.93	3.95	4.22	4.16
20	8.26	7.65	7.77	7.13
21	7.49	6.79	6.94	8.28
22	3.85	2.75	3.07	3.26

[a] IC_{50} is the concentration of inhibitor at which 50% of enzyme activity was inhibited. [b] Data estimated from linear regression for each enzyme using ΔE_{gas} regression values (see Table 7). [c] Juvenile hormone esterase (JHE) from the cabbage looper *Trichoplusia ni*. Data estimated from linear regression for each enzyme using ΔG_{aq}(COSMO) regression values (see Table 7). [d] The predicted IC_{50} values for compounds **12** and **13** are shown here because they differ greatly from experimental values.

estimated using a regression equation and is therefore not a directly measured value.

We subsequently examined the correlations between the calculated log P values and biological potency for both the ketone and *gem*-diol forms of the inhibitors and found little correlation ($R^2 = 0.16$ for the ketone and $R^2 = 0.03$ for the *gem*-diol). After verifying that lipophilicity did not account for our observed trend, we proceeded with the study and selected a subset of our model compounds for synthesis to validate the correlation model (compounds **6**−**13**). Together, this group of compounds rationally extended the structure of the carboxylesterase inhibitors and addressed our two goals for this project: to develop a model for carboxylesterase inhibition that accounted for varying moieties around the carbonyl group and to determine the role of sulfur in increased inhibition potency.

These eight compounds were assayed for inhibition activity against three mammalian enzyme systems and JHE (Tables 5 and 6). Following observation of IC_{50} data, it was determined that compound **12** had a significantly different bimolecular rate constant (k_i) than compounds **6**−**11** (see Kinetic Analysis). This variation in kinetic performance made it inappropriate

Table 7. Regression and Correlation Analysis[a]

enzyme	energy parameter	equation	R^2	r_s [b]	$P(F)$ [c]	p value
human[d]	ΔE_{gas} [e]	$y = -0.39x + 0.23$	0.94	0.98	0.47	<0.01
murine[d]	ΔE_{gas} [e]	$y = -0.43x - 1.28$	0.90	0.98	0.45	<0.01
porcine[d]	ΔE_{gas} [e]	$y = -0.42x - 0.78$	0.84	0.98	0.42	<0.01
JHE[f]	ΔG_{aq}(COSMO) [g]	$y = -0.42x + 6.52$	0.87	0.94	0.42	<0.01

[a] All correlation and regression values for all energy parameters are given in Supporting Information (Table 18). [b] The Spearman−Rank correlation coefficient. [c] F test probability value. [d] $n = 6$ (compounds **6**−**11**). [e] Energy of hydration in the gas phase (kcal/mol). [f] Juvenile hormone esterase, $n = 10$ (compounds **1**−**11**, excluding compound **5**). [g] Free energy of hydration in the aqueous phase using COSMO solvation model (kcal/mol).[52]

to include compound **12** in the correlation analyses. In addition, it was found that compound **13** was unstable under the assay conditions and quickly disproportionated into a number of products, making accurate measurement of the IC$_{50}$ value impossible. All correlation analyses were therefore performed with compounds **6**−**11** for the mammalian enzymes and compounds **1**−**11** for JHE.

Comparison of Energy Values. All four esterase systems examined in this study provided similar results. A notable trend was that all models had a bias toward the prediction of strong inhibitors, with the absolute error increasing with decreasing inhibitor potency. We correlated the measured inhibitory potencies of these compounds with energy to hydrate the ketone to form the corresponding *gem*-diol. We used five different mathematical models to estimate different forms of the hydration energies in these correlations: the gas phase electronic energies (total energy at 0 K excluding vibrational zero-point energy) and free energies, denoted ΔE_{gas} and ΔG_{gas}; the aqueous phase electronic and free energies using the COSMO solvent model, denoted ΔE_{aq} and ΔG_{aq}(COSMO); and the aqueous phase free energies using the Langevin dipole solvation model, denoted ΔG_{aq}(ChemSol). Table 7 shows the strongest linear correlations found between the inhibitory potencies and the hydration energies for each enzyme preparation (the correlations for all hydration energies are shown in Table 18 in Supporting Information). The positive correlations between energy of hydration and biological potency were upheld for all four enzyme preparations with all five energies. The ΔE_{gas} values provided the best correlations in all three mammalian enzyme systems but were only slightly better than the ΔG_{gas} values. The JHE system was quite different in that ΔE_{gas} values provided the poorest correlations and ΔG_{aq}(COSMO) provided the best. It was expected that the free energy values would provide better correlations than the electronic energies because of the inclusion of entropic effects. However, it is unlikely that the small variations between the R^2 values for the electronic and free energies are statistically significant. Inclusion of aqueous solvation effects on the hydration energy by the COSMO and ChemSol models did not improve the correlations. The ChemSol model gave the poorest correlation. This model is in principle more realistic than the COSMO model, given that water molecules are modeled as discrete dipoles surrounding the molecule. However, it is a new method that has not been fully parametrized for sulfur-containing groups,[53] which could explain its somewhat poorer correlation values. All ChemSol free energy values still correlated strongly with inhibitor potency. The calculated energies all correlated very strongly with each other as well, with

Table 8. Correlation Values between Calculated Hydration Energies

	ΔE_{gas} [a]	ΔG_{gas} [b]	ΔE_{aq} [c]	ΔG_{aq} (COSMO)[d]	ΔG_{aq} (ChemSol)[e]
ΔE_{gas}	1.00	0.99	0.97	0.93	0.92
ΔG_{gas}		1.00	0.97	0.96	0.95
ΔE_{aq}			1.00	0.99	0.95
ΔG_{aq}(COSMO)				1.00	0.96
ΔG_{aq}(ChemSol)					1.00

[a] Energy of hydration in the gas phase (kcal/mol). [b] Free energy of hydration in the gas phase (kcal/mol). [c] Energy of hydration in the aqueous phase using the COSMO solvation model (kcal/mol).[52] [d] Free energy of hydration in the aqueous phase using COSMO solvation model (kcal/mol).[52] [e] Free energy of hydration in the aqueous phase using the Langevin dipole (ChemSol) solvation model (kcal/mol).[53]

all correlation coefficients greater than or equal to 0.92 (Table 8). Given the high interrelation coefficients, it appears that any of these models are appropriate for estimating the hydration energy and subsequent biological potency of carboxylesterase inhibitors.

Juvenile Hormone Esterase Activity. JHE correlations were initially performed with 11 compounds including the 5 compounds that were collected from literature sources. However, on the basis of analysis, compound **5** was excluded from the correlation. This compound contains a triple bond in the position α to the carbonyl and has a geometry radically different from the geometries of the other inhibitors used for this correlation.[42] The different geometry could interfere with the mode of binding employed by the other inhibitors in this series, which all contain a bent form of geometry at this point (either tetrahedral sp^3 or trigonal planar sp^2) as opposed to linear (sp). The exclusion of compound **5** had a very significant effect on the correlation values in the gas phase, with the R^2 value for ΔE_{gas} increasing from 0.63 ($P(F) = 0.24$) to 0.82 ($P(F) = 0.38$), whereas the ΔG_{aq}(COSMO) value only increased slightly from 0.85 ($P(F) = 0.41$) to 0.87 ($P(F) = 0.42$). The observed trend showed that aqueous models provided improved regression values over gaseous, and free energy correlations were tighter than electronic correlations. Compound **5** had essentially no effect on the R^2 value for the aqueous free energy calculations, showing that these values were superior at describing inhibitor activity. In this system, these results suggest that the effects of the unsaturation are better modeled in an aqueous environment. The JHE data correlated highly with the mammalian data (Table 9), with all correlation values greater than or equal to 0.97.

Mammalian Carboxylesterase Inhibition. The human liver microsome, mouse liver microsome, and commercial porcine esterase preparations used for carboxylesterase activity analysis were crude preparations likely consisting of multiple isozymes. The porcine

Table 9. Correlation Values for Enzyme Inhibition[a]

	human	murine	porcine	JHE
human	1.00	0.98	0.95	0.98
murine		1.00	0.99	0.99
porcine			1.00	0.97
JHE				1.00

[a] Correlation analysis was performed for compounds **6**–**12**.

esterase preparation undergoes a one-step acetone precipitation purification but still contains multiple esterases.[34,41] It is expected that the individual isozymes respond differently to chemical inhibition, resulting in varying inhibition profiles. In addition, each isozyme would be expected to have a different substrate profile. The substrate *p*-nitrophenyl acetate (PNPA) has been shown to be very nonspecific and is hydrolyzed by a broad range of esterases[2] and was therefore used for all mammalian carboxylesterase assays.

All three mammalian esterase systems examined in this study provided similar results. The positive correlations between energy of hydration and biological potency were upheld for all three enzyme preparations with all five energy parameters (Table 7; and Table 18 in Supporting Information). In addition, the inhibition values were highly correlated among all four enzyme systems (including JHE), with all correlation values greater than or equal to 0.95 (Table 9). One of the aims of this project was to examine the role of the sulfur atom in esterase inhibition. The mammalian esterase assays were conducted with six different inhibitors, four of which contained a sulfur atom. Hammock et al. initially hypothesized that the increased potency of the β-thioether compounds, such as **6**, over the trifluoromethyl ketones, such as **3**, was due to the sulfur mimicking the electronic properties of the 2,3-double bond of juvenile hormone.[36] Although this observation holds for all JHEs so far examined, the higher potency of the thioether-containing compounds on mammalian enzymes whose substrates lack α,β-unsaturated esters does not support application of this hypothesis to esterases in general. All three mammalian enzymes had significant correlations between inhibitor potency and all energy of hydration calculations at the $p < 0.01$ level (except for some porcine esterase values). The effects of sulfur therefore appear to be adequately described by its contribution to ketone hydration. However, further analysis showed that in all mammalian systems the inhibition of sulfur-containing inhibitors was often underestimated, indicating the existence of additional effects not accounted for by contributions to ketone hydration.

One possibility is that the sulfur atom could form associations with amino acid residues in the enzyme that enhance its binding. Morgan and McAdon showed that sulfur is capable of forming interactions with aromatic residues, where interaction is defined as "separated by the sum of their van der Waals' radii, or so close that no other atom can intervene".[66] They found that the maximal allowable separation between the two atoms is 5.0 Å and reported that sulfur–aromatic interactions are energetically favorable. It is therefore feasible that the sulfur atom in these inhibitors could be forming sulfur–aromatic interactions with residues in the active site, which would account for the additional activity of the thioether-containing inhibitors unex-
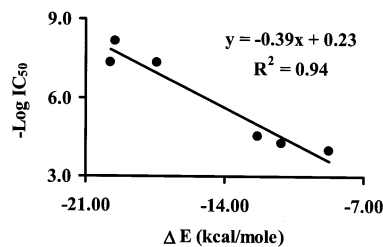
Figure 2. Correlation between inhibition of human liver microsome carboxylesterase activity (the concentration of inhibitor that inhibits 50% of enzyme activity, IC_{50}) and the gas phase electronic energy of hydration (ΔE_{gas}) of the ketone moiety in the enzyme inhibitor ($p < 0.01$). All assays were performed in triplicate, and procedures are explained in the text.

plained by the hydration energies. However, the activity of both sulfone and thioether inhibitors was underpredicted in all of the enzyme systems examined, not just the thioether-containing compounds. It is probable that the sulfone moiety is not capable of forming the same type of sulfur–aromatic interaction as the thioether. Therefore, the additional effects of sulfur are probably exerted by a different mechanism, such as binding effects that are not solely explained by the hydration extent of the ketone moiety. However, these effects appear to be minor compared to the effects of sulfur upon ketone hydration.

We only optimized one parameter in these studies, ketone hydration, and extensive work has been conducted previously to maximize esterase inhibition parameters with TFK inhibitors. Therefore, this study is useful for understanding the mechanism of carboxylesterase inhibition and provides information on an important parameter for QSAR studies, but it does not stand alone as an independent model. For example, previous studies have shown that the hydrophobic alkane tail is very important for activity, and we have used that optimized parameter for all compounds in this study[35,42,43] In addition, there are other models that correlate physical constants with esterase activity. Buchwald and Bodor reported that steric effects surrounding the ester moiety were correlated with ester hydrolysis rates,[24] with the inaccessible solid angle around the sp[2] oxygen ($\Omega_h^{O=}$) of the ester carbonyl having the most significant correlation with the rate of metabolism.[3] It is possible that the steric environment surrounding the carbonyl oxygen of the TFK inhibitors also correlates with inhibition potency, and further research could examine these effects. We also applied our model to electric eel acetylcholinesterase inhibition using data from Székács et al.[35] and found no correlation between ketone hydration state and enzyme inhibition (see Supporting Information for a graphical representation of those results). It therefore appears that this model exhibits some selectivity for carboxylesterases. However, it is necessary to verify this observation with other enzyme systems.

Human Carboxylesterase Activity. The correlations between the five energy values and human liver carboxylesterase inhibition were the strongest of all mammalian systems examined. The electronic energy (ΔE_{gas}) had the strongest correlation with an R^2 value of 0.94 ($p < 0.01$; Figure 2). The aqueous energies (both electronic and Gibbs) also provided good correlations.

The percent error for the predicted potency of all inhibitors was less than 10%, and only the potency of compound **6** was significantly underpredicted. This observation supports previously reported results that the potency of the TFK-containing thioether is greater than predicted by its structure.[41] However, the observed IC$_{50}$ is only 2-fold more potent than the predicted value (see Supporting Information for a list of all predicted values). Interestingly, compound **8**, a thioether-containing compound that has a methyl group in place of the trifluoromethyl group, was overpredicted by the model. It therefore appears that the increase in potency observed with the thioether functions in tandem with the trifluoromethyl group. This effect could be further examined by synthesizing sulfur-containing inhibitors of varying degrees of fluorination on the methyl group α to the ketone.

Murine Carboxylesterase Activity. The results were very similar to the human microsomal data, with ΔE_{gas} giving the best correlation to inhibitor potency with an R^2 of 0.90 ($p < 0.01$). All compounds except **8** and **9** predicted IC$_{50}$ values with less than 10% error. The mouse had a prediction pattern very similar to that of the human preparation, with compound **6** being underpredicted and **8** being overpredicted (35% error). Compound **7** was well predicted, and compound **9** was underpredicted (24% error). These observations do not support the theory that there is some component of the sulfone moiety that interferes with binding. The binding seems to be more a function of the trifluoromethyl group than the sulfone. One possibility is that the trifluoromethyl group itself is interacting with residues in the enzyme active site. To examine those possible effects would require advanced docking analysis using a TFK-containing inhibitor. A crystal structure for rabbit carboxylesterase has recently been published[67] and could be used to examine the potential interactions of the trifluoromethyl group or the sulfone moiety versus the thioether. In addition, there is a homology model of JHE that could be used to probe these effects and compare variations in mammalian versus insect carboxylesterases.[68] These results demonstrate that the esterlytic activity in human and murine systems seems to function with a similar mechanism. This observation provides further justification for the application of murine data to human systems when studying carboxylesterase activity and mechanism of action.

Porcine Carboxylesterase Activity. The porcine esterase assays were conducted with a commercial preparation, thus serving as a benchmark enzyme for comparisons with other research groups. The results paralleled those observed for the other mammalian systems but gave the lowest correlations for any of the mammalian enzyme systems. The correlations generally overestimated inhibitor potency, with four inhibitors predicted to be more potent than observed. This trend was observed for all five calculated energies. The results for compounds **8** and **9** were similar in both the porcine and murine preparations with both showing a very high level of deviation from the value predicted from the calculated hydration energies, 44% and 28%, respectively. It therefore appears that the inhibitory potencies of these two compounds are not well-predicted by their hydration energy. The biological data for porcine es-
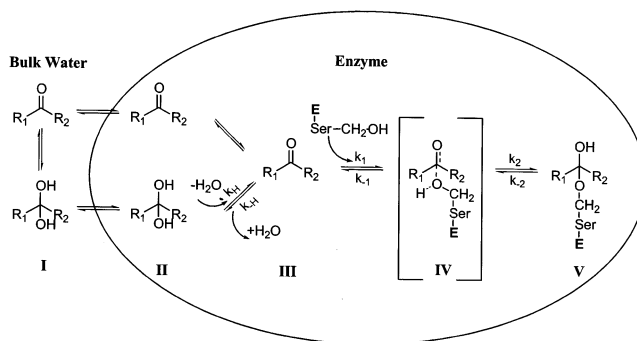
Figure 3. Steps involved in inhibition of the enzyme. This figure shows a possible approach to breaking down the events into four key processes. First, the inhibitor diffuses from the bulk water into the enzyme (**II**). It is not known if the inhibitor is in the ketone or *gem*-diol form at this point. If the inhibitor is hydrated, it now undergoes a dehydration reaction to form the proposed active form of the inhibitor as the ketone (**III**). A nucleophilic serine residue in the active site then attacks the inhibitor, forming an intermediate complex (**IV**), which can either form an inhibited enzyme complex (**V**) or revert to the free inhibitor (**III**). Inhibitors whose structures favor the tetrahedral geometry at the ketone (*gem*-diol form) would be expected to support the bound enzyme complex (**V**), thus resulting in inhibitors of increased potency. However, if the inhibitor structure extremely favors the *gem*-diol, then the k_H reaction could become the rate-limiting step, preventing the formation of the ketone inhibitor (**III**). **E** indicates the enzyme, and Ser is the serine catalytic residue in the enzyme active site with the terminal nucleophilic hydroxyl group.

terase showed that the inhibitors were consistently less potent than for the other mammalian systems. The results for this system were more similar to the JHE data than to the results of other mammalian systems, with a correlation value of 0.97 versus 0.95 for the human microsomal enzyme (Table 9). It therefore appears that caution should be used in applying the results for porcine esterase inhibition studies to other mammalian systems, including humans, since they do not appear to be directly correlated.

Kinetic Analysis. Compound **12** was predicted to be the most potent carboxylesterase inhibitor based on the energy calculations with a −log IC$_{50}$ value for human liver microsomal esterase inhibition of 10.00 (Table 6). However, the observed −log IC$_{50}$ was 6.51 (Table 5), showing almost 4 orders of magnitude difference in inhibition potency. At first, it was assumed that this inhibitor was an exception to the observed correlation between biological potency and energy of hydration. However, the mechanism of esterase inhibition is dependent on several processes (Figure 3). It is assumed that the ketone is the active form of the inhibitor, not the *gem*-diol.[44] Hence, if the compound is hydrated in free solution, then it is necessary for it to first dehydrate to the ketone in order to inhibit the enzyme. The rate of this reaction is described by k_H in Figure 3. It has been shown that fluorinated compounds in aqueous solutions are hydrated between 97% and 100%, whereas the hydration of nonfluorinated ketones is well below 1%.[69] This large degree of ketone hydration was further demonstrated by Scott and Zuman who measured values of k_{-H} for aqueous solutions of α,α,α-trifluoroacetophenone in the range 0.0036−0.018.[70] These hydration levels are qualitatively consistent with the different predicted hydration energies calculated in this study.
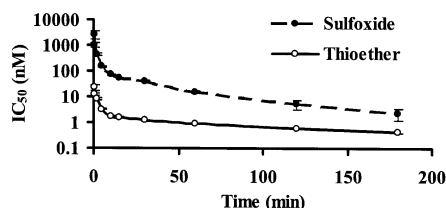
Figure 4. Time dependence of the IC_{50} (concentration of inhibitor that inhibit 50% of enzyme activity) for porcine esterase activity inhibition by compound **6** (thioether) and compound **12** (sulfoxide). Enzyme was incubated with the inhibitor for each time duration, and then activity was measured using the substrate *p*-nitrophenyl acetate (PNPA) visualized at 405 nm with a 2 min kinetic read. All assays were performed in triplicate.

The trifluoromethyl ketone compounds have been reported to be slow tight binding inhibitors.[62] The slow portion of their binding kinetics may be a reflection of the ketone/*gem*-diol equilibrium where their binding kinetics are dominated by the slow k_H. If this hypothesis holds true, then compounds that highly favor their hydrated forms would in effect be poor inhibitors because the concentration of inhibitory ketone would be extremely low. The dehydration step, k_H, would subsequently be the rate-limiting step of binding. To test this hypothesis, we examined the kinetics of the binding of compound **12** and compared it to compound **6**, whose kinetics has been extensively described in earlier publications.[36,62,71]

We performed two experiments to examine the binding kinetics. The first experiment involved measuring the time dependence of the IC_{50}. We measured the IC_{50} of compounds **12** and **6** at several time points and found that the initial IC_{50} for compound **12** at 30 s was >100-fold less potent than compound **6**. However, after a 3 h incubation, the IC_{50} for compound **12** was only 5-fold less potent than compound **6** (Figure 4). It is probable that if the incubation was allowed to proceed for an extended period of time (i.e., >24 h), then the IC_{50} of compound **12** would indeed be more potent than compound **6**. To further examine this point, we measured the bimolecular rate constant (k_i) for binding of the inhibitor to the enzyme. The rate constants provided additional evidence for this hypothesis in that compound **12** had a k_i of 9.5×10^5 M^{-1} min^{-1} as opposed to compound **6** with a k_i of 3.2×10^7 M^{-1} min^{-1} (Figure 5). The large difference in the rate constants demonstrates that compound **12** has different binding kinetics than compound **6**. Compounds **7**−**11** were examined as well and found to have kinetics similar to the kinetics of compound **6**, with essentially full binding occurring by 10 min (data not shown). On the basis of these analyses, it was decided that it was not appropriate to include compound **12** in the correlation analyses using the short time scale enzyme inhibition data. However, the kinetic behavior of the compound does further support the hypothesis that inhibition potency is related to the degree of ketone hydration.

It appears that there is a limit to the favorable effects of increased ketone hydration on potency. If a ketone is highly hydrated, then k_{-H} is the dominant factor and formation of the ketone inhibitor is limited. However, if the ketone is not polarized, then k_1 will be the limiting factor for the nucleophilic attack of the catalytic serine.
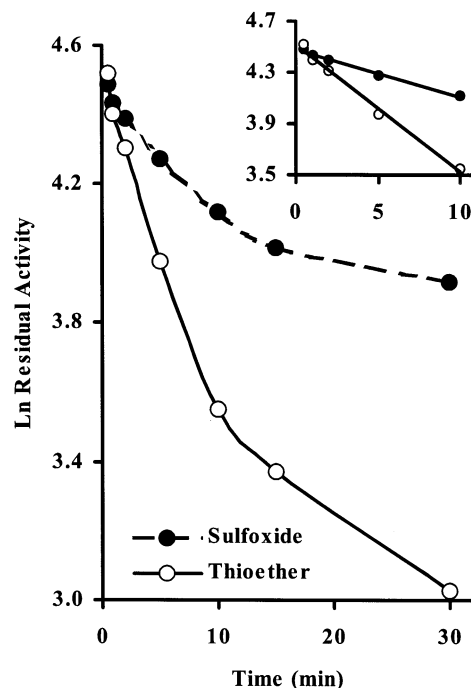
Figure 5. Pseudo-first-order plots for the inhibition of porcine esterase activity by compound **6** (thioether) and compound **12** (sulfoxide) at final molar concentrations of 3.1 and 39.1 nM, respectively. The inset shows the linear portion from 0.5 to 10 min that was used to calculate the second-order rate constants (k_i) of 3.2×10^7 M^{-1} min^{-1} ($R^2 = 0.99$) for thioether (**6**) and 9.5×10^5 M^{-1} min^{-1} ($R^2 = 0.98$) for sulfoxide (**12**). Each point represents the mean of three separate determinations. The axes units for the inset graph are identical to those of the primary graph.

The optimal inhibitor may be a balance between k_H and k_1. On the basis of the observed enzyme inhibition data, it appears that compound **6**, the thioether, is the optimal inhibitor in this series. It is sufficiently polarized to undergo nucleophilic attack by the serine, yet it is not so polarized as to retard ketone formation. Further attempts to verify this process could be performed by enriching the carbonyl carbon with ^{13}C and monitoring the hydration state of the ketone by ^{13}C NMR as it binds to the enzyme.

Carbonyl Charge Calculations. The charge on the carbonyl carbon atom of each inhibitor in the ketone form was calculated and correlated with inhibitor potency. It was hypothesized that compounds that favor the *gem*-diol state would also have a decreased atomic charge on the carbonyl carbon due to the electron-withdrawing nature of the surrounding chemical moieties. The atomic charge values should therefore strongly correlate with inhibition results just as for the energy calculations. Buchwald and Bodor reported that the charge on the carbonyl carbon affected the rate of ester hydrolysis and was useful for predicting ester half-lives in human blood.[3] The data for all four enzymes are very similar and are summarized in Table 10. The atomic charge data cluster into two groups represented by the trifluoromethyl-containing inhibitors (compounds **6**, **7**, and **10**) and the methyl-containing inhibitors (compounds **8**, **9**, and **11**). These data are not statistically significant because of the clustering of the points, and only qualitative interpretations are valid. It would be necessary to synthesize compounds of varying degrees

Table 10. Regression and Correlation Analyses for Calculated Atomic Charge on Inhibitor Carbonyl Carbon

enzyme	equation	R^2	r_s [a]	$P(F)$ [b]	p value
human[c]	$y = 34.46x - 24.17$	0.94	0.97	0.47	<0.01
murine[c]	$y = 39.47x - 26.04$	0.93	0.97	0.47	<0.01
porcine[c]	$y = 38.38x - 25.68$	0.89	0.95	0.45	<0.01
JHE[d]	$y = 23.71x - 17.06$	0.58	0.76	0.20	>0.05
JHE[e]	$y = 40.11x - 26.16$	0.94	0.97	0.47	<0.01

[a] The Spearman–Rank correlation coefficient. [b] F test probability value. [c] $n = 6$ (compounds **6**–**11**). [d] $n = 11$ (compounds **1**–**11**). [e] $n = 9$ (compounds **1**–**11**, except compounds **4** and **5**).

$$y = -34.46x + 24.18$$
$$R^2 = 0.94$$
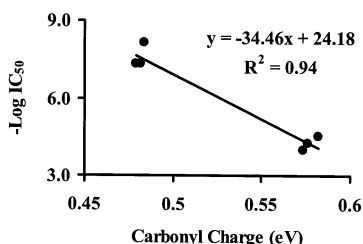
Figure 6. Correlation between inhibition of human liver microsome carboxylesterase activity (the concentration of inhibitor that inhibits 50% of enzyme activity, IC_{50}) and the calculated partial atomic charge of the ketone carbon atom of the enzyme inhibitor ($p < 0.01$). All assays were performed in triplicate as described in the text.

of fluorination in order to map out the region between the two clusters. We found that the carbonyl carbon charges correlated well with the calculated energies, with free energy values giving the strongest correlation (for ΔG_{aq}, $R^2 = 0.93$; for ΔG_{aq}(COSMO), $R^2 = 0.91$; for ΔG_{aq}(ChemSol), $R^2 = 0.95$) and electronic energies providing slightly weaker correlations (for ΔE_{aq}, $R^2 = 0.86$; for ΔE_{gas}, $R^2 = 0.88$). The more thermodynamically relevant free energy term had a stronger correlation with carbonyl carbon charge in both the gas and aqueous states, indicating that entropic effects are also important for this relationship. The correlation results are graphically displayed in the Supporting Information.

The inhibition of human liver esterlytic activity correlated most strongly with atomic charge on the carbonyl carbon, giving an R^2 of 0.94 (Figure 6), with the murine enzyme preparation essentially the same with an R^2 of 0.93. The porcine enzyme did not correlate as well but still had a relatively strong correlation ($R^2 = 0.89$). JHE gave the most interesting response out of the four enzymes studied. The initial correlation was performed with compounds **1**–**11** and gave a poor regression with an R^2 of 0.58. There were two main outliers, compounds **4** and **5**, which are both unsaturated compounds. The estimated charge on the inhibitor carbonyl carbon was much lower than would be predicted by the biological activity. It therefore appears that the effects of unsaturation upon carbonyl hydration are less than calculations would predict. This observation is particularly interesting in light of the fact that the alkene compound (**4**) was shown to be a more potent inhibitor than its energy calculations predicted. This observation was attributed to the unsaturation mimicking the unsaturation in juvenile hormone, the natural substrate for JHE. However, even with this additional factor, the alkene inhibitor potency is poorly predicted by atomic charge. Compounds **4** and **5** therefore behaved similarly, even though **5** was not designed as a mimic of juvenile hormone. These results demonstrate that
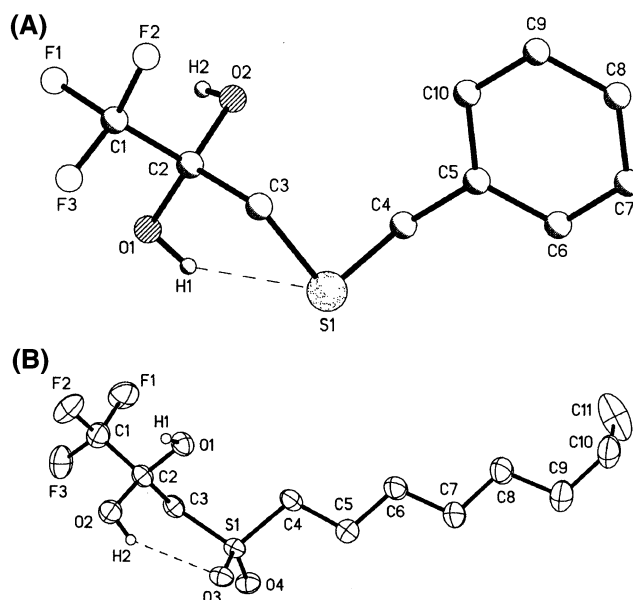
Figure 7. (A) Crystal structure of 1,1,1-trifluoro-5-phenyl-4-thiapentane-2,2-diol. The structure shows the presence of a 2.37 Å intramolecular hydrogen bond between the sulfur atom and a hydroxy group of the *gem*-diol. Data were taken from Olmstead et al.[72] (Cambridge Crystallographic Data Centre deposition number "FORFUN"). (B) Crystal structure of 1,1,1-trifluoro-3-(octane-1-sulfonyl)·propane-2,2-diol (**26**). The structure shows the presence of a 2.34 Å intramolecular hydrogen bond between an oxygen atom of the sulfone moiety and a hydroxy group of the *gem*-diol (Cambridge Crystallographic Data Centre deposition number "CCDC 178195"). See Supporting Information for the crystallographic coordinates.

there could be additional effects influencing the degree of ketone hydration for unsaturated systems or alternatively the unsaturation is interacting with other residues in the active site. However, the calculations give an excellent estimation of the activity for saturated systems (compounds **6**–**11**).

Intramolecular Hydrogen Bond Studies. A number of researchers have theorized that the presence of an intramolecular hydrogen bond between the hydrated ketone (*gem*-diol) and the sulfur atom β to the ketone could play a role in inhibitor potency through the stabilization of the *gem*-diol or the tetrahedral enzyme inhibitor complex (Figure 7).[34,35,42] We therefore evaluated the role, if any, of this hydrogen bonding in inhibition potency. Olmstead et al. had previously shown that an internal hydrogen bond existed in the crystal structure of the carboxylesterase inhibitor 1,1,1-trifluoro-5-phenyl-4-thiapentane-2,2-diol.[72] We therefore knew that the bond existed in thioether-containing compounds in the crystalline state. In a previous project, we had synthesized a sulfone analogue of the thioether compound that was also a crystalline solid.[34] We obtained a crystal structure of this compound to examine if the intramolecular hydrogen bond was also present in the sulfone analogue. A comparison of the two compounds, the thioether and the sulfone, enabled us to examine the potential role of the intramolecular hydrogen bond in inhibitor potency.

The compound 1,1,1-trifluoro-3-(octane-1-sulfonyl)-propane-2,2-diol (**26**) was selected for crystal structure determination. It had crystals that were finer and more "needlelike" than 1,1,1-trifluoro-3-(hexane-1-sulfonyl)-

propane-2,2-diol (**7**) and were readily crystallized from a 50:50 mixture of *n*-butyl chloride and hexanes. Crystals of **26** crystallized with two molecules in the asymmetric unit. The two molecules differed in the conformation of the terminal methyl group of the octyl chain, giving torsion angles of −68° and 179° for molecules 1 and 2, respectively. Each molecule had one intramolecular hydrogen bond that is depicted for molecule 1 (Figure 7B). In addition, there is intermolecular hydrogen bonding between each molecule and its inversion-related pair. The crystal packing of the molecules places hydrophilic and hydrophobic ends in proximity (see Supporting Information for a full listing of the atomic coordinates for all atoms in the assigned structure of **26**).

We had thus demonstrated that the intramolecular hydrogen bond existed in both the sulfone and thioether compounds (in the crystalline state). We hypothesized that the *gem*-diol would be capable of forming a stronger hydrogen bond with the oxygen of the sulfone than with the sulfur of the thioether. Oxygen is well-known to form stronger hydrogen bonds than sulfur.[73] However, some evidence has shown that sulfur is capable of forming relatively strong hydrogen bonds in certain environments.[73] Another factor was that the sulfone compound formed a six-membered ring whereas the thioether compound formed a five-membered ring. We therefore had multiple effects occurring, and it was uncertain which effect would have the dominant role. The biological data for inhibition of carboxylesterase activity in human microsomes showed that the thioether compound (**6**) was more potent than the sulfone compound (**7**). This trend was consistent in the other three esterase systems examined in this study (Table 5). These observations were also supported by the ab initio energy calculations.

On the basis of this evidence, it appeared that the hydrogen bond was not playing a significant role. We, however, wanted to examine this effect more precisely. We therefore performed a series of ab initio calculations to determine the strength of the intramolecular hydrogen bond in compounds **6** and **7** in different physical environments ranging from gas-like to aqueous. The calculations varied by the dielectric constant of the medium in which the compounds were modeled. Since it is difficult to know the exact nature of the physicochemical environment inside the enzyme, the calculations were performed with a range of solvent dielectric values. The results vary with the solvent, but the magnitude of difference in the strength of the bond between the two systems did not change greatly (Figure 8). The strength of the hydrogen bond in the sulfone compound was only slightly stronger than that in the thioether and varies from twice as strong in the gas phase to approximately three times as strong in the aqueous phase. The COSMO method gave a 3-fold greater strength of the hydrogen bond in the sulfone compound, whereas the ChemSol method showed that the bond strengths were essentially equal in the two compounds.

Given that the active site of the enzyme is probably neither fully aqueous-like nor fully gas-like, benzene and methanol were chosen as two other solvents to model the bond strengths. We suspect that benzene is
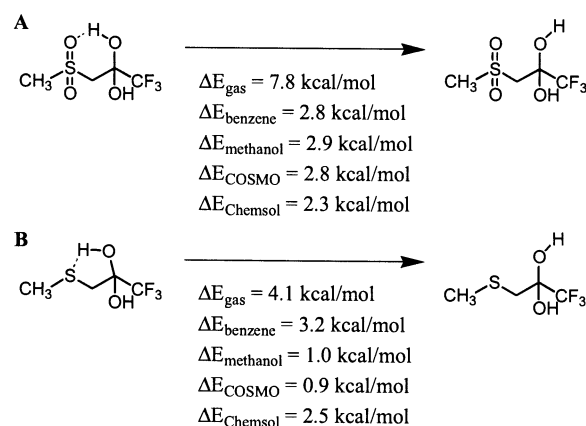
Figure 8. Results for ab initio calculations of intramolecular hydrogen bond strength of sulfone-containing (A) and thioether-containing (B) carboxylesterase inhibitors. The alkyl chain was approximated by a methyl group to reduce the required computational time. Calculations were performed in five different environments: the gaseous state; methanol, benzene, and the aqueous state using two different methods; the conductor-like screening solvation model (COSMO) method;[52] and the Langevin dipole (ChemSol) method.[53] Calculations were performed using the energy required to break the hydrogen bond between a hydroxyl group of the *gem*-diol and either a sulfone oxygen (A) or the sulfur of the thioether (B).

a more realistic representation of the physicochemical parameters within the active site given its intermediate properties between gas and aqueous phases as well as its mimicking of aromatic residues within the enzyme. The effects evidenced with the benzene calculations predictably fall between those of the gas and aqueous phases. However, in this case, hydrogen bonding in the thioether compound was approximately 10% stronger than that in the sulfone (3.2 kcal/mol for the thioether versus 2.8 kcal/mol for the sulfone). These differences in bond strength are not very pronounced and as such support our observations that the biological potency of the thioether and sulfone compounds can be mainly explained through their contributions to the hydration state of the ketone. Therefore, any effects of these two moieties upon activity are probably not exerted through the formation of an internal hydrogen bond. However, our data support the hypothesis that a hydrogen bond is capable of forming with the sulfur atom present in these inhibitors. While our data suggest that an intramolecular hydrogen bond involving sulfur does not contribute strongly to inhibitor potency, it is possible that a hydrogen bond forms between the sulfur and residues in the enzyme active site. As mentioned before, this phenomenon would have to be studied on an enzyme-specific basis and would require enzymatic structural information such as a crystal structure, or at least a homology model, with which to conduct docking studies.

Synthesis. Data for compounds **1**−**6** were collected from literature sources and were not synthesized for this work.[35,36] On the basis of the results of energy calculations, a series of molecules of varying potency were chosen to test the models. The selenium-containing inhibitors were not synthesized because of the potential for selenium toxicity and difficulty in obtaining the required starting materials. Attempts to synthesize compound **20** were unsuccessful, with the direct reaction of amines with 1-bromo-3,3,3-trifluroropropan-2-one

Scheme 1. Synthesis of Ether-Containing Carboxylesterase Inhibitors (DMP Is the Dess–Martin Periodinane)
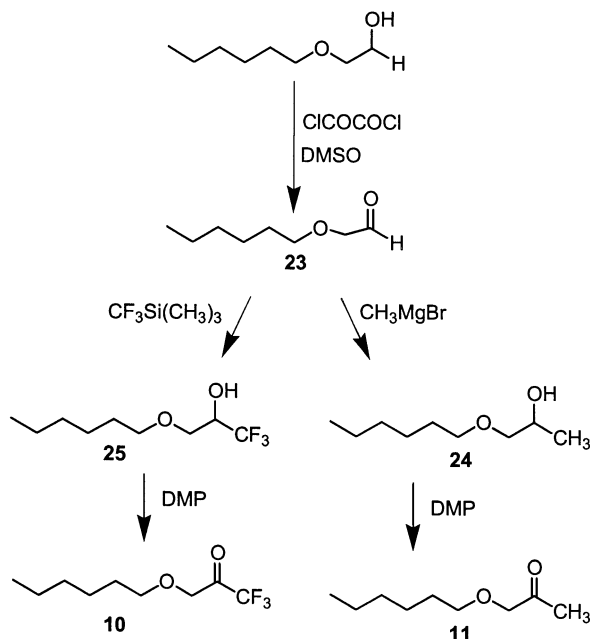
resulting in cyclic products. The synthesis of compound **10** proved to be difficult, and several different methods were attempted before the successful one reported in this study. Initially, hexanol was directly treated with 1-bromo-3,3,3-trifluroropropan-2-one, using methods of Johnstone and Rose.[74] A number of catalysts were then attempted including ZnI_2 and $AgClO_4$ as well as formation of the alkylate anion using NaH and CaH_2. A DMSO/KOH system was also attempted, all without success. The same series of reactions was also used in an attempt to synthesize compound **11** using chloroacetone instead of 1-bromo-3,3,3-trifluroropropan-2-one, again with no success. The syntheses of **10** and **11** were finally achieved by oxidizing hexyloxyethanol to the aldehyde (**23**), followed by methylation (**24**) and oxidation of the resultant alcohol to the ketone for **11** or trifluoromethylation to form **25** and oxidation of the alcohol to the ketone for **10** (Scheme 1).

The synthesis of **10** always resulted in formation of the *gem*-diol compound as evidenced by the broad OH singlet by ^1H NMR (D_2O exchangeable). Several unsuccessful attempts were made to dehydrate the compound, including use of $MgSO_4$, $CaCl_2$, and molecular sieves in $CHCl_3$. This tendency of electron-deficient carbonyls to hydrate has been reported earlier with the sulfur derivates of these compounds.[34–36]

A number of obstacles were experienced in the synthesis of compound **12**. The sulfoxide-selective oxidation was difficult to achieve because it was important to ensure that no sulfone was synthesized as a byproduct. Attempts to use H_2O_2 as the oxidizing agent according to methods of Drabowicz and Mikolajczyk[75] were unsuccessful and resulted in multiple byproducts. The use of *m*-chloroperoxybenzoic acid (*m*-CPBA) has been extensively referenced for oxidation reactions, including the formation of sulfoxides and sulfones[76] (and references therein). We found that it was extremely difficult to effect the selective conversion of thioether to sulfoxide using published procedures.[77] Syntheses

always resulted in some sulfone production. It was therefore necessary to use a smaller amount of oxidizing agent than predicted. The maximum acceptable amount was 0.5 mmol of *m*-CPBA per 1.0 mmol of thioether (**6**). Additionally, it was found that compound **12** was not thermally stable. The compound decomposed into the starting thioether and free thiol, as well as disulfide, when examined by GC/EI-MS (injection port at 250 °C). Analysis by LC/ESI-MS was used to confirm the structure of **12**, and time course analyses showed that the compound was completely stable in both ethanolic and aqueous solutions with no measurable degradation after several days. While the dehydration product dominated the spectra, the molecular ion was detectable.

The same problems as with compound **12** were experienced with the synthesis of compound **13**. It was possible to increase the molar equivalents of *m*-CPBA to 0.85 mmol of *m*-CPBA per 1.0 mmol of thioether (**8**), resulting in selective sulfoxide formation. However, compound **13** was not stable and quickly degraded under ambient conditions. The rate of degradation was enhanced greatly in nucleophilic solvents such as methanol, ethanol, acetonitrile, and water. Interestingly, the compound was stable by GC/EI-MS analysis but quickly degraded under LC/ESI-MS analysis or in aqueous systems (see Supporting Information for additional data on the synthesis of compounds **12** and **13** and a graphical representation of the dependence of sulfur oxidation on the molar amount of *m*-CPBA).

Conclusion

For a set of esterase inhibitors chosen to minimize variance in lipophilicity and to maximize variance in electronic characteristics of the reactive carbonyl, we were able to correlate biological potency with both the charge on the carbonyl carbon and the hydration energy of the ketone. These results provide insight into the mechanism of esterase inhibition by polarized ketone-containing inhibitors. This evidence supports earlier suggestions that inhibitors that favor tetrahedral geometry (i.e., hydrated ketones) exert their increased potency by favoring the tetrahedral geometry of the inhibitor-bound enzyme complex (a transition-state analogue). However, data indicate that there is the potential to have an inhibitor that is "too hydrated", and we provide evidence that the highly hydrated inhibitors are very slow tight binders because of the decreased concentration of the ketone (which we assume to be the active form of the inhibitor). It is still unclear which species, the *gem*-diol or the ketone, is the active inhibitor. If the ketone is the inhibitor, which most studies seem to suggest, then the key step in enzyme inhibition becomes the dehydration to the ketone. These results also demonstrate that the enhanced role of sulfur in esterase inhibition can be largely attributed to its effects upon ketone hydration. Additionally, our results indicate that intramolecular hydrogen bonding between the *gem*-diol of the hydrated ketone and the sulfur atom does not account for the increased potency of sulfur-containing inhibitors. Results showed that in this case murine liver microsome esterlytic activity is an appropriate model for human liver microsome esterlytic activity, with the two systems exhibiting similar inhibition profiles and correlations with inhibitor parameters.

However, a porcine system did not correlate nearly as well with either the murine or human systems and had responses that were more similar to the insect enzyme JHE. The mammalian models consistently provided better correlations in the gas phase, and the JHE model had slightly better correlations in the aqueous phase. However, the differences were small enough to prohibit specific comments regarding potential differences within the physicochemical parameters among these enzymes. In summary, we have employed quantum chemical calculations to elucidate a mechanism for the inhibition of esterases. Results from this study should be useful in designing esterase-activated prodrugs and soft drugs as well as in understanding the mechanism of action of carboxylesterases.

Experimental Section

CAUTION! *The Dess−Martin periodinane has been reported to be explosive upon impact or at temperatures above 200 °C. Proper care should be used in the handling and storage of this compound.*

General. All work was conducted under an inert atmosphere (either N_2 or Ar) in oven-dried glassware. Reaction solvents were dehydrated when necessary in accordance with standard protocols. Reaction progress and product purity were assessed on 10 cm F_{254} silica thin-layer chromatography (TLC) plates (250 μm thickness, EM Science; Gibbstown, NJ) visualized with either phosphomolybdic acid and heating or 2,4-dinitrophenylhydrazine. Purity was initially assayed by the number of spots responding to the visualization agents and the lack of UV-sensitive spots at 254 nm, confirming the removal of UV-active impurities. Flash column chromatography was performed on silica gel (Merck Kieselgel 60). Yields for all reactions were not optimized. Unless stated otherwise, all materials were obtained from commercial suppliers and were used without further purification.

Structural characterization and purity were provided by ^{1}H NMR, ^{13}C NMR, ^{19}F NMR (Mercury 300, Varian; Palo Alto, CA), GC/EI-MS, LC/ESI-MS, HPLC, and LC/TOF-MS. For GC analysis, samples were analyzed on an HP 6890 GC (Agilent Technologies; Engelwood, CO) equipped with a 30 m DB-17MS column (J&W Scientific; Folsom, CA) with a 0.25 mm internal diameter and a 0.25 μm film thickness with a He carrier gas at a flow rate of 0.8 mL/min. The injector temperature was 250 °C, and the initial column temperature was 50 °C and was held for 5.00 min and then ramped at 15 °C/min to 320 °C and held for 2.00 min. The GC was interfaced with an HP 5973 mass spectrometer that was run in full-scan mode from 50 to 550 m/z with a quadrupole temperature of 186 °C and a source temperature of 240 °C. Electron ionization (EI) fragmentation patterns supported all reported structures. Mass spectra as well as total ion chromatograms (TIC) are provided in Supporting Information. LC/ESI-MS analysis was performed with a Micromass Quattro Ultima (Manchester, U.K.) mass spectrometer in negative mode coupled to a Waters 2790 liquid chromatograph (Milford, MA). The mass spectrometer cone voltage was set at 50 V with a capillary voltage of 3.0 kV, using a scan range of 50−300 m/z and a 3 s scan time. All ESI mass spectral data supported the proposed structures.

Compound purity was assessed by HPLC using two different systems. Method A used a Spherisorb ODS 5 μm 4.6 × 250 mm C-18 column (Waters) and a Waters 600 solvent delivery system with an HP 1100 variable-wavelength UV detector (Agilent Technologies). The system was run at a flow rate of 1 mL/min with a linear gradient of 100% solvent A (20% ACN and 80% H_2O) to 100% solvent B (100% ACN) in 80 min and then 100% B for 20 min. Data collection was performed with Waters Millennium[32] chromatography manager. Method B employed a Brownlee Spheri-5 5 μm 4.6 × 220 mm cyanopropyl column and a Waters 680 gradient controller equipped with a Waters 510 gradient solvent delivery system with an HP 1050 variable-wavelength detector. The system was run a flow rate

of 1 mL/min with a linear gradient of 100% solvent A (H_2O) to 50% solvent B (50% MeOH and 50% H_2O) in 80 min and then 50% B for 20 min. Both detection systems were run at 205 nm and revealed a single UV absorbing peak. Analysis at 254 nm resulted in no detectable impurities. These data are provided in Table 17A in Supporting Information.

High-resolution mass spectrometry (HRMS) was performed on an LCT orthogonal time-of-flight mass spectrometer (TOF/MS, Micromass UK Limited; Manchester, U.K.). The mass spectrometer was operated with MassLynx 3.5 software. The spectrometer was equipped with a Z-flow electrospray ionization source, and sodium trifluoroacetate was used for external multipoint calibration.[78] Mass accuracy was typically better than 10 ppm, and resolution was typically better than 4500 full width at half-maximum (fwhm). The system was operated at a flow rate of 25 μL/min. Data were acquired in either negative (Table 17B in Supporting Information) or positive mode (Table 17C in Supporting Information) depending on the compound, with the following parameters: capillary 2880 V, sample cone 30 V, RF lens 250 V, extraction cone 10 V, acceleration 180 V, pusher cycle time 50 s^{-1}, ion energy 30 V, and reflectron 1794 V. The analog−digital converter was operated at 3.6 GHz frequency. The reported spectra represent the averages of 20−40 consecutive spectra. MassLynx software was used for all data processing and mass measurement determinations.

All compounds were >97% purity as evidenced by TLC, GC/EI-MS, HPLC, NMR, and a sharp melting point when appropriate (see Table 17A in Supporting Information for complete purity assessment of all compounds). Melting point data were collected with a Thomas-Hoover apparatus (A. H. Thomas Co.; Philadelphia, PA) and are uncorrected. Due to the hygroscopic nature of these compounds, it was not possible to obtain accurate elemental analyses for purity assessment. This observation has been reported by other authors for compounds of similar structure.[29,34]

Hexyloxyethanal (23). A solution of oxalyl chloride (85 mmol, 7.4 mL) in CH_2Cl_2 (150 mL) was cooled to −70 °C in a dry ice/EtOH bath (the internal temperature was kept below −60 °C throughout the reaction and subsequent workup). A solution of DMSO (179 mmol, 12.7 mL) in CH_2Cl_2 (20 mL) was then added dropwise. After gas evolution had completely subsided (1 h), 2-hexyloxyethanol (66 mmol, 9.60 g) in CH_2Cl_2 (10 mL) was added to the mixture. After 30 min, triethylamine (180 mmol, 25 mL) was added dropwise, and the resultant white suspension was stirred for an additional 30 min. The cooling bath was then removed, and the internal temperature was raised to 0 °C. Ice-cold 3 N aqueous HCl (200 mL) was poured slowly into the reaction mixture with vigorous stirring to give a clear two-phase solution. The phases were separated, and the water phase was extracted with CH_2Cl_2 (50 mL). The combined organic extract was washed with 1 N aqueous HCl (2 × 100 mL), saturated aqueous $NaHCO_3$ (100 mL), and brine (100 mL). This solution was dried over $MgSO_4$, filtered, and stripped under reduced pressure. The residual yellow oil was purified by distillation (bp 50 °C, 3 mmHg) to provide **23** as a colorless oil (49 mmol, 7.03 g, 74% yield). ^{1}H NMR ($CDCl_3$) δ (ppm) 0.90 (t, J = 6.8 Hz, 3H), 1.3−1.4 (m, 6H), 1.6−1.7 (m, 2H), 3.53 (t, J = 6.6 Hz, 2H), 4.06 (s, 2H), 9.74 (s, 1H); ^{13}C NMR δ (ppm) 14.0, 22.6, 25.7, 29.5, 31.6, 72.3, 76.3, 201.2; single spot by TLC (hexanes/EtOAc, 80:20); GC/EI-MS m/z [M]$^+$ = 144.1 (<1%), [M − CHO]$^+$ = 115.1 (33%), [M − C_3H_7O]$^+$ = 101.1 (4%), [M − $C_2H_3O_2$]$^+$ = 85.1 (58%); LC/ESI-MS m/z calculated for [M] = 144.1, observed [M − H]$^-$ = 143.1.

1-Hexyloxypropan-2-ol (24). Compound **23** (21 mmol, 3.00 g) in THF (5 mL) was added to a 0.92 M solution of methylmagnesium bromide in THF (28 mmol, 30 mL) dropwise at 0 °C. After the mixture was stirred for 30 min, 1 N aqueous HCl (40 mL) was slowly added with vigorous stirring. The bulk of the THF was then removed by rotary evaporation. The resultant two-phase mixture was extracted with Et_2O (3 × 25 mL), and the combined extract was washed with saturated aqueous $NaHCO_3$ (50 mL) and brine (50 mL). This solution was dried over $MgSO_4$ and filtered, and the solvent was

stripped under reduced pressure. The residual oil was purified by distillation (bp 57 °C, 1 mmHg) to afford **24** as a colorless oil (14 mmol, 2.32 g, 70% yield). ^{1}H NMR (CDCl$_3$) δ (ppm) 0.89 (m, 3H), 1.14 (d, $J = 6.4$ Hz, 3H), 1.30 (m, 6H), 1.58 (m, 2H), 2.4 (broad s, 1H), 3.20 (dd, $J = 9.4$, 8.3 Hz, 1H), 3.41 (dd, $J = 9.4$, 3.1 Hz, 1H), 3.47 (m, 2H), 3.96 (ddq, $J = 3.1$, 8.3, 6.4 Hz, 1H); ^{13}C NMR (CDCl$_3$) δ (ppm) 14.0, 18.6, 22.6, 25.8, 29.6, 31.6, 66.4, 71.4, 76.2; single spot by TLC (hexanes/EtOAc, 80:20); GC/EI-MS m/z [M]$^+$ = 160.3 (<1%), [M − CH$_3$]$^+$ = 145.1 (2%), [M − C$_3$H$_7$O]$^+$ = 101.1 (3%), [M − C$_3$H$_6$O$_2$]$^+$ = 85.1 (45%); LC/ ESI-MS m/z calculated for [M] = 160.1, observed [M − H]$^-$ = 159.1.

1-Hexyloxypropan-2-one (11). The Dess−Martin periodinane (DMP) was prepared according to standard methods[79,80] and added (28 mmol, 5.82 g) to a solution of compound **24** (12 mmol, 2.00 g) in CH$_2$Cl$_2$ (30 mL) at room temperature, and the solution was stirred overnight. The resultant cloudy solution was diluted with Et$_2$O (150 mL), washed with 10% w/v aqueous Na$_2$S$_2$O$_3$ (100 mL, saturated with NaHCO$_3$), and brine (100 mL), and dried over MgSO$_4$. After the solution was filtered and concentrated, the residual oil was purified by distillation (bp 53 °C, 1 mmHg) to give **11** as a colorless oil (8.6 mmol, 1.36 g, 69% yield). ^{1}H NMR (CDCl$_3$) δ (ppm) 0.89 (t, $J = 6.9$ Hz, 3H), 1.3−1.4 (m, 6H), 1.6−1.7 (m, 2H), 2.16 (s, 3H), 3.48 (t, $J = 6.6$ Hz, 2H), 4.02 (s, 2H); ^{13}C NMR (CDCl$_3$) δ (ppm) 14.0, 22.6, 25.7, 26.3, 29.5, 31.7, 72.0, 76.4, 207.5; single spot by TLC (hexanes/EtOAc, 80:20); GC/EI-MS m/z [M]$^+$ = 158.1 (<1%), [M − C$_2$H$_3$O]$^+$ = 115.1 (4%), [M − C$_3$H$_5$O$_2$]$^+$ = 85.1 (76%); LC/ ESI-MS m/z calculated for [M] = 158.1, observed [M − H]$^+$ = 159.1; TOF HRMS calculated for [M + H]$^+$ = 159.1385, observed 159.1407.

1,1,1-Trifluoro-3-hexyloxypropan-2-ol (25). A catalytic amount (~20 mg) of cesium fluoride was added to a solution of **24** (20 mmol, 2.95 g) and (trifluoromethyl)trimethylsilane (21 mmol, 3.10 g) in THF (35 mL) according to the methods of Singh et al.[81] After the evolution of heat had subsided (~1 h), aqueous 3 N HCl (50 mL) was added and the mixture was vigorously stirred for 1 h. After the THF was removed by rotary evaporation, the aqueous residue was extracted with Et$_2$O (2 × 70 mL). The combined extracts were washed with brine (100 mL) and dried over MgSO$_4$. The resulting solution was filtered and stripped under reduced pressure to give an oil that was purified by flash column chromatography (hexane/EtOAc,12:1) to afford **25** as a colorless oil (16 mmol, 3.50 g, 80% yield). ^{1}H NMR (CDCl$_3$) δ (ppm) 0.89 (t, $J = 6.9$ Hz, 3H), 1.3−1.4 (m, 6H), 1.5−1.6 (m, 2H), 2.9 (broad s, 1H, D$_2$O exchangeable), 3.51 (t, $J = 6.6$ Hz, 2H), 3.61 (dd, $J = 6.1$, 10.1 Hz, 1H), 3.68 (ddq, $J = 10.1$, 3.8, 0.8 Hz, 1H), 4.11 (m, 1H); ^{13}C NMR (CDCl$_3$) δ (ppm) 14.0, 22.6, 25.6, 29.4, 31.6, 67.9, 69.3 (q$_{CCF}$, $J = 30$ Hz), 72.1, 124.2 (q$_{CF}$, $J = 292$ Hz); ^{19}F NMR (CDCl$_3$) δ (ppm) −78.24 (d, $J = 6.0$); single spot by TLC (hexanes/EtOAc, 80:20); GC/EI-MS m/z [M]$^+$ = 214.2 (<1%), [M − C$_6$H$_{13}$0]$^+$ = 113.0 (25%), [M − C$_3$H$_4$O$_2$F$_3$]$^+$ = 85.1 (95%), [M − C$_8$H$_{17}$O$_2$]$^+$ = 69.0 (25%); LC/ ESI-MS m/z calculated for [M] = 214.1, observed [M − H]$^-$ = 213.1.

1,1,1-Trifluoro-3-hexyloxypropane-2,2-diol (10). The DMP, synthesized according to standard methods,[79,80] was added (7 mmol, 2.97 g) to a solution of compound **25** (5 mmol, 1.00 g) in CH$_2$Cl$_2$ (16 mL) at room temperature, and the solution was stirred overnight. The resultant cloudy solution was diluted with Et$_2$O (100 mL), washed with 10% w/v aqueous Na$_2$S$_2$O$_3$ (100 mL, saturated with NaHCO$_3$) and brine (100 mL), and dried over MgSO$_4$. After the solution was filtered and concentrated, the residual oil was purified by flash column chromatography (hexane/EtOAc, 4:1) to give **10** as a colorless oil (4.2 mmol, 0.90 g, 85% yield). ^{1}H NMR (CDCl$_3$) δ (ppm) 0.89 (t, $J = 6.8$ Hz, 3H), 1.3−1.4 (m, 6H), 1.6−1.7 (m, 2H), 3.6 (m, 3.3H), 3.79 (broad s, 1.6H, exchangeable by D$_2$O); ^{13}C NMR (CDCl$_3$) δ (ppm) 14.0, 22.5, 25.5, 29.4, 31.5, 69.6, 71.4 (q$_{CCF}$, $J = 105$ Hz), 72.8, 122.5 (q$_{CF}$, $J = 285$ Hz); ^{19}F NMR (CDCl$_3$) δ (ppm) −78.34 (s, 32%), −85.73 (s, 68%); single spot by TLC (hexanes/EtOAc, 80:20); GC/EI-MS m/z [M − H$_2$O]$^+$ = 212.1 (<1%), [M − H$_2$O − C$_2$OF$_3$]$^+$ = 115.1 (22%), [M − H$_2$O − C$_3$H$_2$O$_2$F$_3$]$^+$ = 85.1 (75%), [M − H$_2$O − C$_8$H$_{15}$O$_2$]$^+$ = 69.0 (30%);

LC/ ESI-MS m/z calculated for [M − H$_2$O]$^-$ = 212.1, observed [M − H$_2$O−H]$^-$ = 211.1; TOF HRMS calculated for [M − H$_2$O − H]$^-$ = 211.0946, observed 211.0945.

1-Hexylsulfanylpropan-2-one (8). 1-Hexanethiol (82.5 mmol, 11.7 mL) was added to a stirring mixture of potassium carbonate (11.4 g) in CCl$_4$ (20 mL). Chloroacetone (75 mmol, 6 mL) was added dropwise over 10 min, followed by the catalytic addition of 1,8-diazabicyclo[5.4.0]undec-7-ene (DBU). The reaction was allowed to proceed overnight under a gentle stream of N$_2$. The reaction mixture was quenched with Et$_2$O (20 mL) and washed with saturated aqueous NaHCO$_3$ (3 × 50 mL). The organic fraction was dried over MgSO$_4$ and filtered, and the solvent was stripped under reduced pressure. The mixture was purified by distillation (bp 59 °C, 0.5 mmHg) to give a colorless oil (46.2 mmol, 8.1 g, 56% yield). ^{1}H NMR (CDCl$_3$) δ 0.86 (t, $J = 6.7$ Hz, 3H), 1.26 (m, 4H), 1.34 (m, 2H), 1.54 (m, $J = 7.6$ Hz, 2H), 2.28 (s, 3H), 2.46 (t, $J = 7.1$ Hz, 2H), 3.18 (s, 2H); ^{13}C NMR (CDCl$_3$) δ 14.26, 22.76, 27.87, 28.65, 29.16, 31.58, 32.34, 42.23, 204.30; single spot by TLC (hexanes/EtOAc, 80:20); GC/EI-MS m/z [M]$^+$ = 174.1 (24%), [M − C$_2$H$_3$O]$^+$ = 131.1 (14%), [M − C$_3$H$_5$O]$^+$ = 117.1 (15%); LC/ ESI-MS ions not observed in positive or negative mode; TOF HRMS calculated for [M + H]$^+$ = 175.1156, observed 175.1113.

1-(Hexane-1-sulfonyl)propan-2-one (9). Compound **8** (4.4 mmol, 0.77 g) was added to a stirring solution of CHCl$_3$ (50 mL), followed by m-chloroperoxybenzoic acid (70−75%, 11.6 mmol, 2.7 g). After 30 min, the reaction was worked up according to methods of Wheelock et al.[34] It was not necessary to further purify the final product, which had an overall yield of 77%. ^{1}H NMR (CDCl$_3$) δ 0.92 (t, $J = 6.5$ Hz, 3H), 1.32 (m, 4H), 1.45 (m, 2H), 1.84 (q, $J = 6.5$ Hz, 2H), 2.44 (s, 3H), 3.11 (t, $J = 7.3$ Hz, 2H), 4.03 (s, 3H); ^{13}C NMR (CDCl$_3$) δ 13.87, 21.75, 22.23, 27.90, 31.08, 32.02, 53.41, 63.63, 197.40; single spot by TLC (hexanes/EtOAc, 80:20); GC/EI-MS m/z [M − C$_3$H$_5$O]$^+$ = 149.1 (21%), [M − C$_3$H$_5$O$_2$]$^+$ = 131.1 (2%), [M − C$_3$H$_5$O$_3$S]$^+$ = 85.1 (23%); LC/ESI-MS m/z calculated for [M] = 206.1, observed [M − H]$^-$ = 205.1; TOF HRMS calculated for [M − H]$^-$ = 205.0899, observed 205.0913.

1-(Hexane-1-sulfinyl)propan-2-one (13). m-CPBA (70−75%, 0.43 mmol, 100 mg) was added to **8** (0.50 mmol, 87 mg) with stirring in CH$_2$Cl$_2$ (50 mL) at 0 °C. The reaction was allowed to proceed for 1 h, and the mixture was brought up to room temperature using adapted methods of Ando et al.[77] The mixture was then washed with saturated NaHCO$_3$ (3 × 50 mL) and brine (50 mL), dried with MgSO$_4$, filtered, and stripped under reduced pressure. The crude mixture was recrystallized from hexanes to give white needlelike crystals of **13** (0.41 mmol, 77 mg, 81% yield). Mp = 55−57 °C; ^{1}H NMR (CDCl$_3$) δ 0.92 (t, $J = 6.2$ Hz, 3H), 1.28 (m, 4H), 1.41 (m, 2H), 1.72 (m, 2H), 2.31 (s, 3H), 2.73 (m, 2H), 3.72 (dd, $J = 13.5$, 29.9 Hz, 2H); ^{13}C NMR (CDCl$_3$) δ 14.16, 22.56, 22.72, 28.57, 31.51, 32.73, 52.89, 63.06, 200.61; single spot by TLC (hexanes/EtOAc, 80:20); GC/EI-MS m/z [M + H]$^+$ = 191.1 (1%), [M + H − O]$^+$ = 173.1 (84%), [M − C$_3$H$_5$O]$^+$ = 133.1 (27%), [M − C$_3$H$_5$O$_2$S]$^+$ = 85.1 (19%); not stable by LC/ ESI-MS analysis.

1,1,1-Trifluoro-3-hexylsulfanylpropan-2-one (6). Compound **6** was synthesized according to the methods of Wheelock et al. and is not further reported here.[34] ^{1}H NMR (CDCl$_3$) δ 0.87 (t, $J = 6.7$ Hz, 3H), 1.28 (m, 4H), 1.37 (m, 2H), 1.57 (m, 2H), 2.50 (t, $J = 7.3$ Hz, 2H), 3.48 (s, 2H); ^{13}C NMR (CDCl$_3$) δ 13.94, 22.46, 28.27, 28.49, 31.25, 31.92, 34.76, 115.51 (q$_{CCF}$, $J = 35$ Hz), 185.01 (q$_{CF}$, $J = 292$ Hz); ^{19}F NMR (CDCl$_3$) δ −76.30 (s); single spot by TLC (chloroform/ethanol, 95:5); GC/EI-MS m/z [M]$^+$ = 228.1 (34%), [M − C$_2$OF$_3$]$^+$ = 131.1 (67%), [M − C$_3$H$_2$OF$_3$]$^+$ = 117.1 (100%); LC/ ESI-MS m/z calculated for [M]$^-$ = 228.1, observed [M − H]$^-$ = 227.1; TOF HRMS calculated for [M − H]$^-$ = 227.0718, observed 227.0708.

1,1,1-Trifluoro-3-(hexane-1-sulfonyl)propane-2,2-diol (7). Compound **7** was synthesized according to methods of Wheelock et al.[34] with a minor adaptation. Compound **6** was oxidized with m-CPBA for 1 h instead of the 48 h reported. This length of time was sufficient for full oxidation to the sulfone in >99% conversion. The remaining procedure was performed as previously published. ^{1}H NMR (CDCl$_3$) δ 0.89

(t, $J = 6.7$ Hz, 3H), 1.31 (m, 4H), 1.42 (m, 2H), 1.85 (m, 2H), 3.33 (m, 2H), 3.39 (s, 2H), 5.23 (broad s, 1.6H, D_2O exchangeable); ^{13}C NMR ($CDCl_3$) δ 14.13, 21.87, 22.50, 28.14, 31.31, 52.77, 56.40, 92.01 (q_{CCF}, $J = 34$ Hz), 121.78 (q_{CF}, $J = 287$ Hz); ^{19}F NMR ($CDCl_3$) δ −79.26, (s, 3%), −87.17 (s, 97%); single spot by TLC (chloroform/ethanol, 95:5); GC/EI-MS m/z [M − H_2O]$^+$ = 260.1 (<1%), [M − H_2O − $C_3H_2OF_3$]$^+$ = 149.1 (16%), [M − H_2O − $C_6H_{13}O_2S$]$^+$ = 111.0 (23%); LC/ ESI-MS m/z calculated for [M − H_2O]$^-$ = 260.1, observed [M − H_2O − H]$^-$ = 259.1; TOF HRMS calculated for [M − H_2O − H]$^-$ = 259.0616, observed 259.0597.

1,1,1-Trifluoro-3-(hexane-1-sulfinyl)propan-2-one (12). *m*-CPBA (70−75%, 0.75 mmol, 175 mg) was dissolved in CH_2-Cl_2 (10 mL) and was washed with saturated $NaHCO_3$ (50 mL) to remove the *m*-chlorobenzoic acid degradation product. This solution was then added dropwise over 20 min to a solution of **6** (1.5 mmol, 344 mg) and $NaHCO_3$ (~2.4 mmol, 200 mg) in CH_2Cl_2 (50 mL) at 0 °C. The reaction was allowed to proceed for 1 h and then brought up to room temperature and worked up as for **13** to give a viscous yellow liquid. Approximately 1−2 mL of hexanes was added, which initiated precipitation of a white solid. This solid was recrystallized from a mixture of hexanes and *n*-butyl chloride (50:50) to give a white powdery solid (0.44 mmol, 90 mg, 29% yield). Mp = 79−80 °C; ^1H NMR ($CDCl_3$) δ 0.91 (t, $J = 7.0$ Hz, 3H), 1.33 (m, 4H), 1.47 (m, 2H), 1.78 (m, 2H), 2.88 (m, 2H), 3.03 (m, 2H), 4.88 (broad s, 0.8 H, D_2O exchangeable), 6.35 (broad s, 0.8 H, D_2O exchangeable); ^{13}C NMR ($CDCl_3$) δ 14.18, 22.42, 22.58, 28.53, 31.47, 50.36, 53.31; ^{19}F NMR ($CDCl_3$) δ −79.56 (s, 4%), −87.63 (s, 96%); single spot by TLC (chloroform/ethanol, 95:5); compound was not thermally stable but was detected among various degradation products by GC/EI-MS m/z [M]$^+$ = 244.1 (<1%), [M − H − O]$^+$ = 227.1 (29%), [M − CF_3]$^+$ = 175.1 (2%), [M − C_3H_2-OF_3]$^+$ = 133.1 (8%); LC/ ESI-MS m/z calculated for [M − H_2O]$^-$ = 244.1, observed [M − H_2O − H]$^-$ = 243.1.

1,1,1-Trifluoro-3-(octane-1-sulfonyl)propane-2,2-diol (26). Compound **26** (Figure 7B) was synthesized using the same procedures as for compound **7**. The final product was recrystallized from *n*-butyl chloride to give white needlelike crystals in 94% yield. Mp = 87−88 °C; ^1H NMR ($CDCl_3$) δ 0.88 (t, $J = 6.45$ Hz, 3H), 1.29 (broad m, 10H), 1.87 (m, 2H), 3.33 (m, 2H), 3.39 (s, 2H), 4.79 (broad s, 1.5H, D_2O exchangeable); ^{13}C NMR ($CDCl_3$) δ 13.96, 21.72, 22.53, 28.24, 28.41, 28.88, 31.64, 52.57, 56.27, 91.88 (q_{CCF}, $J = 33$ Hz), 121.78 (q_{CF}, $J = 286$ Hz); ^{19}F NMR ($CDCl_3$) δ −79.21 (s, 3%), −87.29 (s, 97%); single spot by TLC (chloroform/ethanol, 95:5); GC/EI-MS m/z [M − H_2O]$^+$ = 288.1 (<1%), [M − H_2O − $C_3H_2OF_3$]$^+$ = 177.1 (28%), [M − H_2O − $C_8H_{17}O_2S$]$^+$ = 111.0 (10%); LC/ ESI-MS m/z calculated for [M − H_2O]$^-$ = 288.1, observed [M − H_2O − H]$^-$ = 287.1.

X-ray Structure Determination of 1,1,1-Trifluoro-3-(octane-1-sulfonyl)propane-2,2-diol (26). A colorless plate of dimensions 0.80 mm × 0.16 mm × 0.02 mm was mounted in the 130 K nitrogen cold stream provided by a Siemens LT-2 low-temperature apparatus on the goniometer head of a Siemens P4 diffractometer. Diffraction data were collected with nickel-filtered Cu Kα radiation supplied by a Siemens rotating anode to a maximum 2Θ of 112°. A total of 4528 reflections were collected in the range +*h*, +*k*, ±*l*, of which 3888 were unique (*R*(int)=0.032) and 2888 were observed ($I > 2\sigma(I)$). The structure was solved by direct methods (SHELXS-97[FN1], version 5.10, Bruker Analytical X-ray Instruments, Inc.; Madison, WI) and refined by full-matrix least-squares on F^2 (SHELXL-97[FN1]). All non-hydrogen atoms were refined with anisotropic thermal parameters. Hydrogen atoms were added by geometry and refined using a riding model except for the hydroxyl hydrogens, which were located on a difference map and refined with a constrained O−H distance of 0.84(1) Å. The maximum and minimum peaks in the final difference Fourier map corresponded to 0.50 and −0.31 e Å^{-3}. The refinement converged with a wR2 value of 0.124 using all data and an R1 value of 0.045 for observed data using 361 parameters, 4 restraints, GOF = 1.04. Crystal Data: $C_{11}H_{21}F_3O_4S$, M = 306.34, monoclinic, $P2_1/c$, $a = 31.750(5)$ Å, $b = 5.3684(8)$ Å, $c = 18.409(3)$ Å, $\beta = 106.583(14)°$, $Z = 8$.

Enzyme Assays. Juvenile Hormone Esterase (JHE) Activity. JHE activity assays were conducted by the methods of Sparks and Hammock[61] as described in Wheelock et al.[34] Briefly, *Trichoplusia ni* larvae were harvested on day 2 of the fifth instar, and hemolymph was collected and diluted 1:1 with 0.1 M sodium phosphate buffer (pH 7.4) containing ~0.5 mmol of phenylthiourea. The diluted enzyme had a specific activity of 1.0 nmol of juvenile hormone III min^{-1} mg^{-1} protein and was frozen at −80 °C. JHE activity was measured with a partition assay based on the hydrolysis of [^{3}H] juvenile hormone III ([^{3}H] JH III). Hemolymph was diluted 300-fold in sodium phosphate buffer (pH 7.4, 0.1 M, 0.1 mg/mL bovine serum albumin) and incubated with inhibitor stock dilutions for 10 min at 30 °C. All inhibitor dilutions were prepared in ethanol, and total ethanol concentration in the assay never exceeded 2% of the total volume. The substrate [^{3}H] JH III was then added for a final concentration of 5 μM and incubated for 15 min at 30 °C. Following incubation, 50 μL of a MeOH/water/ammonium hydroxide solution (10:9:1) was added. The mixture was extracted with 250 μL of isoctane, and a 50 μL aliquot of the aqueous phase was counted by a Wallac 1409 liquid scintillation counter (Wallac; Turku, Finland).

Mammalian Carboxylesterase Activity. Carboxylesterase activity assays were conducted according to the methods of Wheelock et al.[34] and are only briefly described here. Assays were performed in 96-well microtiter styrene flat-bottom plates (Dynex Technologies, Inc.; Chantilly, VA) at 30 °C using *p*-nitrophenyl acetate (PNPA) as the substrate. Inhibitor stock solutions were prepared in ethanol and used at concentrations that never exceeded more than 1% of the total assay volume. Total assay volume was 200 μL in sodium phosphate buffer (pH 7.4, 0.1 M). Enzyme was incubated with the inhibitor for 5 min unless otherwise noted, and then the substrate was added for a final concentration of 0.5 mM followed by optical density analysis at 405 nm on a microplate reader (Spectramax 200, Molecular Devices; Sunnyvale, CA). Protein concentrations were determined using the Pierce BCA protein assay (Pierce; Rockford, IL) with bovine serum albumin as the standard.

Human Carboxylesterase Activity. Human liver microsomes were purchased from Gentest (Woburn, MA; lot no. 17, catalog no. 452161). Microsomes were prepared from 16 individuals (10 males, 6 females) and were partially characterized for P450 activity and pathogenicity. Donor information for each individual as well as P450 activity and pathogenicity data can be obtained directly from Gentest (http://www-.gentest.com/index.html) using the above-supplied catalog and lot numbers. Microsomes were solubilized as described for the murine liver microsomes and stored at −80 °C until use. Activity assays were performed as described above using 3.1 μg of protein per well.

Murine Carboxylesterase Activity. Murine liver microsomal carboxylesterase activities were performed with solubilized microsomes prepared by methods adapted from literature procedures.[34,39,82] Sixteen week-old male Swiss−Webster mice were purchased from Charles River Breeding Laboratory (Hollister, CA) and were 30−35 g upon receipt. Mice were housed in HEPA-filtered racks for 7 d before use and were fed and watered ab libitum with a light cycle of 12 h of light and 12 h of darkness. Animal care procedures were approved by the Animal Use and Care Committee at the University of California, Davis. After 1 week, mice were sacrificed by carbon dioxide asphyxiation and livers were immediately excised, rinsed in a 1.15% KCl solution (w/v), homogenized on ice with a Polytron homogenizer (Brinkman Instruments; Westbury, NY), and centrifuged at 10000*g* for 20 min at 4 °C. Supernatant fractions were further centrifuged at 100000*g* for 60 min. The resulting pellet was resuspended and recentrifuged at 100000*g* for an additional 60 min. This pellet was then resuspended in sodium phosphate buffer (pH 7.4, 0.1 M) for a final protein concentration of 10.9 mg/mL and frozen at −80 °C. Microsomes were then solubilized with 1%

n-octyl-β-D-glucopyranoside (Sigma Chemical Co.) and diluted with additional sodium phosphate buffer to give a final concentration of 0.42 mg/mL. Solubilized microsomes were then dialyzed against sodium phosphate buffer for 48 h at 4 °C to remove the detergent. Activity assays were performed as described above using 0.88 μg of total protein per well.

Porcine Carboxylesterase Activity. Porcine carboxylesterase (EC 3.1.1.1) was purchased from Sigma Chemical Co. (catalog no. E-3019). Working solutions of enzyme were prepared at 0.02 mg of protein/mL in sodium phosphate buffer (pH 7.4, 0.1 M) for an activity of 0.3 units/mL (one unit will hydrolyze 1.0 μmol of butyrate to butyric acid and ethanol at pH 8.0 at 25 °C). Assays were conducted as described above using 0.2 μg of protein per well.

Enzyme Inhibition Measurement. The concentration of inhibitor required to reduce enzyme activity by 50% (IC$_{50}$) was determined using the same method for all enzymes.[34] A minimum of five data points, each point resulting from at least three individual analyses, were used to determine the IC$_{50}$. Inhibitor concentrations were adjusted such that the linear region of the curve had at least two points above the IC$_{50}$ and two points below.

Partition Coefficient Measurements. Partition coefficients were determined according to the methods of Leo et al.[64] as described in Thomas et al.[65] Briefly, the target compound was dissolved in cyclohexane (0.1 M) and gently shaken with an equal volume of water for 12 h at room temperature. The quantity of compound in the aqueous phase was quantified by GC/EI-MS under the conditions described above. A solvent regression equation was used to calculate the partitioning into octanol,

$$\log K_{O/W} = 0.941 \log K_{C/W} + 0.69$$

where $K_{O/W}$ represents the partition coefficients for the octanol/water system and $K_{C/W}$ represents those for the cyclohexane/water system.

Statistical Analysis. Statistical analyses were performed using the data analysis module of Microsoft Excel (Microsoft; Redmond, WA). Spearman's coefficients were taken from Siegel.[83]

Supporting Information Available: Crystallographic coordinates for 1,1,1-trifluoro-3-(octane-1-sulfonyl)propane-2,2-diol (**26**) and additional data that include calculated quantum chemical data for all compounds, correlations between carbonyl carbon charge and calculated energies, correlations between acetylcholinesterase activity and calculated energies, predicted IC$_{50}$ values for inhibitors synthesized in this study, purity and GC/EI-MS data for synthesized compounds, and a graphical representation of the dependence of sulfur oxidation on molar quantity of m-CPBA. This material is available free of charge via the Internet at http://pubs.acs.org.

References

(1) Ollis, D. L.; Cheah, E.; Cygler, M.; Dijkstra, B.; Frolow, F.; et al. The α/β hydrolase fold. *Protein Eng.* **1992**, *5*, 197−211.

(2) Satoh, T.; Hosokawa, M. The mammalian carboxylesterases: From molecules to functions. *Annu. Rev. Pharmacol. Toxicol.* **1998**, *38*, 257−288.

(3) Buchwald, P.; Bodor, N. Structure-based estimation of enzymatic hydrolysis rates and its application in computer-aided retrometabolic drug design. *Pharmazie* **2000**, *55*, 210−217.

(4) Pindel, E. V.; Kedishvili, N. Y.; Abraham, T. L.; Brzezinski, M. R.; Zhang, J.; et al. Purification and cloning of a broad substrate specificity human liver carboxylesterase that catalyzes the hydrolysis of cocaine and heroin. *J. Biol. Chem.* **1997**, *272*, 14769−14775.

(5) Stampfli, H. F.; Quon, C. Y. Polymorphic metabolism of flestolol and other ester containing compounds by a carboxylesterase in New Zealand white rabbit blood and cornea. *Res. Commun. Mol. Pathol. Pharmacol.* **1995**, *88*, 87−97.

(6) Yang, H. S.; Wu, W. M.; Bodor, N. Soft drugs. XX. Design, synthesis, and evaluation of ultra-short acting beta-blockers. *Pharm. Res.* **1995**, *12*, 329−336.

(7) Roxburgh, C. J.; Ganellin, C. R.; Athmani, S.; Bisi, A.; Quaglia, W.; et al. Synthesis and structure−activity relationships of Cetiedil analogues as blockers of the Ca^{2+}-activated K$^+$ permeability of erythrocytes. *J. Med. Chem.* **2001**, *44*, 3244−3253.

(8) Brzezinski, M. R.; Spink, B. J.; Dean, R. A.; Berkman, C. E.; Cashman, J. R.; et al. Human liver carboxylesterase hCE-1: binding specificity for cocaine, heroin, and their metabolites and analogs. *Drug Metab. Dispos.* **1997**, *25*, 1089−1096.

(9) Bourland, J. A.; Martin, D. K.; Mayersohn, M. Carboxylesterase-mediated transesterification of meperidine (Demerol) and methylphenidate (Ritalin) in the presence of [^{2}H$_6$] ethanol: preliminary in vitro findings using a rat liver preparation. *J. Pharm. Sci.* **1997**, *86*, 1494−1496.

(10) Cook, C. S.; Karabatsos, P. J.; Schoenhard, G. L.; Karim, A. Species dependent esterase activities for hydrolysis of an anti-HIV prodrug glycovir and bioavailability of active SC-48334. *Pharm. Res.* **1995**, *12*, 1158−1164.

(11) Van de Waterbeemd, H.; Testa, B.; Marrel, C.; Cooper, D. R.; Jenner, P.; et al. Multivariate statistical analysis of L-DOPA esters as potential anti-Parkinsonian prodrugs. *Drug Des. Delivery* **1987**, *2*, 135−143.

(12) Tang, B. K.; Kalow, W. Variable activation of lovastatin by hydrolytic enzymes in human plasma and liver. *J. Clin. Pharmacol.* **1995**, *47*, 449−451.

(13) Senter, P. D.; Marquardt, H.; Thomas, B. A.; Hammock, B. D.; Frank, I. S.; et al. The role of rat serum carboxylesterase in the activation of paclitaxel and camptothecin prodrugs. *Cancer Res.* **1996**, *56*, 1471−1474.

(14) Khanna, R.; Morton, C. L.; Danks, M. K.; Potter, P. M. Proficient metabolism of irinotecan by a human intestinal carboxylesterase. *Cancer Res.* **2000**, *60*, 4725−4728.

(15) Senter, P. D.; Beam, K. S.; Mixan, B.; Wahl, A. F. Identification and activities of human carboxylesterases for the activation of CPT-11, a clinically approved anticancer drug. *Bioconjugate Chem.* **2001**, *12*, 1074−1080.

(16) Weirdl, M.; Morton, C. L.; Weeks, J. K.; Danks, M. K.; Harris, L. C.; et al. Sensitization of human tumor cells to CPT-11 via adenoviral-mediated delivery of a rabbit liver carboxylesterase. *Cancer Res.* **2001**, *61*, 5078−5082.

(17) Lolli, M. L.; Cena, C.; Medana, C.; Lazzarato, L.; Morini, G.; et al. A new class of ibuprofen derivatives with reduced gastrotoxicity. *J. Med. Chem.* **2001**, *44*, 3463−3468.

(18) Jewell, W. T.; Miller, M. G. Identification of a carboxylesterase as the major protein bound by molinate. *Toxicol. Appl. Pharmacol.* **1998**, *149*, 226−234.

(19) Mikhailov, A. T.; Torrado, M. Carboxylesterase overexpression in the male reproductive tract: a universal safeguading mechanism? *Reprod., Fertil. Dev.* **1999**, *11*, 133−145.

(20) van Pelt, J. F.; Moshage, H. J.; Depla, E.; Verhave, J. P.; Yap, S. H. Identification of human liver carboxylesterase as one of the proteins involved in *Plasmodium falciparum* malaria sporozoite invasion in primary cultures of human hepatocytes. *J. Hepatol.* **1997**, *27*, 688−698.

(21) Casida, J. E.; Gammon, D. W.; Glickman, A. H.; Lawrence, L. J. Mechanisms of selective action of pyrethroid insecticides. *Annu. Rev. Pharmacol. Toxicol.* **1983**, *23*, 413−438.

(22) Wallace, T. J.; Ghosh, S.; Grogan, W. M. Molecular cloning and expression of rat lung carboxylesterase and its potential role in the detoxification of organophosphorus compounds. *Am. J. Respir. Cell Mol. Biol.* **1999**, *20*, 1201−1208.

(23) Gupta, R. C.; Dettbarn, W. D. Role of carboxylesterases in the prevention and potentiation of *N*-methylcarbamate toxicity. *Chem. Biol. Interact.* **1993**, *87*, 295–303.

(24) Buchwald, P.; Bodor, N. Quantitative structure–metabolism relationships: Steric and nonsteric effects in the enzymatic hydrolysis of noncongener carboxylic esters. *J. Med. Chem.* **1999**, *42*, 5160–5168.

(25) Bodor, N.; Buchwald, P. Soft drug design: General principles and recent applications. *Med. Res. Rev.* **2000**, *20*, 58–101.

(26) Molinoff, P. B.; Ruddon, R. W. *Goodman & Gilman's the pharmacological basis of therapeutics*, 9th ed.; Hardman, J. G., Limbird, L. E., Eds.; McGraw-Hill: New York, 1996; p 1905.

(27) Quinn, D. M. Esterases of the α/β hydrolase fold family. *Biotransformation*; Elsevier Science: Oxford, 1997; pp 243–264.

(28) Quinn, D. M. Ester hydrolysis. *Enzymes, Enzyme Mechanisms, Proteins, and Aspects of NO Chemistry*; Elsevier Science: Oxford, 1999; pp 101–137.

(29) Nair, H. K.; Lee, K.; Quinn, D. M. *m*-(*N*,*N*,*N*-Trimethylammonio)trifluoroacetophenone: A femtomolar inhibitor of acetylcholinesterase. *J. Am. Chem. Soc.* **1993**, *115*, 9939–9941.

(30) Amour, A.; Reboud-Ravaux, M.; de Rosny, E.; Abouabdellah, A.; Begue, J. P.; et al. Stereoselective synthesis of peptidyl trifluoromethyl alcohols and ketones: Inhibitory potency against human leucocyte elastase, cathepsin G, porcine pancreatic elastase and HIV-1 protease. *J. Pharm. Pharmacol.* **1998**, *50*, 593–600.

(31) Veale, C. A.; Bernstein, P. R.; Bohnert, C. M.; Brown, F. J.; Bryant, C.; et al. Orally active trifluoromethyl ketone inhibitors of human leukocyte elastase. *J. Med. Chem.* **1997**, *40*, 3173–3181.

(32) Edwards, P. D.; Andisik, D. W.; Bryant, C. A.; Ewing, B.; Gomes, B.; et al. Discovery and biological activity or orally active peptidyl trifluoromethyl ketone inhibitors of human neutrophil elastase. *J. Med. Chem.* **1997**, *40*, 1876–1885.

(33) Boger, D. L.; Sato, H.; Lerner, A. E.; Austin, B. J.; Patterson, J. E.; et al. Trifluoromethyl ketone inhibitors of fatty acid amide hydrolase: A probe of structural and conformational features contributing to inhibition. *Bioorg. Med. Chem. Lett.* **1999**, *9*, 265–270.

(34) Wheelock, C. E.; Severson, T. F.; Hammock, B. D. Synthesis of new carboxylesterase inhibitors and evaluation of potency and water solubility. *Chem. Res. Toxicol.* **2001**, *14*, 1563–1572.

(35) Székács, A.; Bordás, B.; Hammock, B. D. Transition state analog enzyme inhibitors: Structure–activity relationships of trifluoromethyl ketones. *Rational Approaches to Structure, Activity, and Ecotoxicology of Agrochemicals*; CRC Press: Boca Raton, FL, 1992; pp 219–249.

(36) Hammock, B. D.; Wing, K. D.; McLaughlin, J.; Lovell, V. M.; Sparks, T. C. Trifluoromethylketones as possible transition state analog inhibitors of juvenile hormone esterase. *Pestic. Biochem. Physiol.* **1982**, *17*, 76–88.

(37) Wolfenden, R. Transition state analogues for enzyme catalysis. *Nature* **1969**, *223*, 704–705.

(38) Lienhard, G. E. Enzymatic catalysis and transition-state theory. *Science* **1973**, *180*, 149–154.

(39) Huang, T. L.; Shiotsuki, T.; Uematsu, T.; Borhan, B.; Li, Q. X.; et al. Structure–activity relationships for substrates and inhibitors of mammalian liver microsomal carboxylesterases. *Pharm. Res.* **1996**, *13*, 1495–1500.

(40) Brodbeck, U.; Schweikert, K.; Gentinetta, R.; Rottenberg, M. Fluorinated aldehydes and ketones acting as quasi-substrate inhibitors of acetylcholinesterase. *Biochim. Biophys. Acta* **1979**, *567*, 357–369.

(41) Ashour, M. B. A.; Hammock, B. D. Substituted trifluoroketones as potent, selective inhibitors of mammalian carboxylesterases. *Biochem. Pharmacol.* **1987**, *36*, 1869–1879.

(42) Linderman, R. J.; Upchurch, L.; Lonikar, M.; Venkatesh, K.; Roe, R. M. Inhibition of insect juvenile hormone esterase by α,β-unsaturated and α-acetylenic trifluoromethyl ketones. *Pestic. Biochem. Physiol.* **1989**, *35*, 291–299.

(43) Linderman, R. J.; Leazer, J.; Venkatesh, K.; Roe, R. M. The inhibition of insect juvenile hormone esterase by trifluoromethylketones: steric parameters at the active site. *Pestic. Biochem. Physiol.* **1987**, *29*, 266–277.

(44) Roe, R. M.; Anspaugh, D. D.; Venkatesh, K.; Linderman, R. J.; Graves, D. M. A novel geminal diol as a highly specific and stable in vivo inhibitor of insect juvenile hormone esterase. *Arch. Insect Biochem. Physiol.* **1997**, *36*, 165–179.

(45) Linderman, R. J.; Jamois, E. A. A semi-empirical and ab initio analysis of fluoroketones as reactive electrophiles. *J. Fluorine Chem.* **1991**, *53*, 79–91.

(46) Linderman, R. J.; Tennyson, S. D.; Schultz, D. A. Comparative stability of fluoroketone hemi-thio acetals, ketals and hydrates. *Tetrahedron Lett.* **1994**, *35*, 6437–3440.

(47) Jensen, F. *Introduction to Computational Chemistry*; John Wiley and Sons: New York, 1999.

(48) Becke, A. D. Density-functional thermochemistry. III. The role of exact exchange. *J. Chem. Phys.* **1993**, *98*, 5648–5652.

(49) Lee, C.; Yang, W.; Parr, R. G. Development of the Colle–Salvetti correlation-energy formula into a functional of the electron density. *Phys. Rev. B* **1988**, *37*, 785–789.

(50) Schüürmann, G.; Cossi, M.; Barone, V.; Tomasi, J. Prediction of the pK_a of carboxylic acids using the ab initio continuum-solvation model PCM-UAHF. *J. Phys. Chem. A* **1998**, *102*, 6706–6712.

(51) Tran, N. L.; Colvin, M. E. The prediction of biochemical acid dissociation constants using first principles quantum chemical simulations. *J. Mol. Struct.: THEOCHEM* **2000**, *532*, 127–137.

(52) Barone, V.; Cossi, M. Quantum calculation of molecular energies and energy gradients in solution by a conductor solvent model. *J. Phys. Chem.* **1998**, *102*, 1995–2001.

(53) Florián, J.; Warshel, A. Langevin dipoles model for ab initio calculations of chemical processes in solution: Parametrization and application to hydration free energies of neutral and ionic solutes and conformational analysis in aqueous solution. *J. Phys. Chem. B* **1997**, *101*, 5583–5595.

(54) Luzhkov, V.; Warshel, A. Microscopic models for quantum-mechanical calculations of chemical processes in solutions–LD/AMPAC and SCAAS/AMPAC calculations of solvation energies. *J. Comput. Chem.* **1992**, *13*, 199–213.

(55) Reed, A. E.; Weinstock, R. B.; Weinhold, F. Natural population analysis. *J. Chem. Phys.* **1985**, *83*, 735–746.

(56) *AMPAC*, version 6.55; Semichem Inc.: Kansas City, MO, 1999.

(57) Tolls, J.; van Dijk, J.; Verbruggen, E. J. M.; Hermens, J. L. M.; Loeprecht, B.; et al. Aqueous solubility–molecular size relationships: A mechanistic case study using C-10- to C-19-alkanes. *J. Phys. Chem. A* **2002**, *106*, 2760–2765.

(58) Hout, R. F., Jr.; Levi, B. A.; Hehre, W. J. Effect of electron correlation on theoretical vibrational frequenies. *J. Comput. Chem.* **1982**, *3*, 234–250.

(59) Frisch, M. J.; Trucks, G. W.; Schlegel, H. B.; Scuseria, G. E.; Robb, M. A.; Cheeseman, J. R.; Zakrzewski, V. G.; Montgomery, J. A., Jr.; Stratmann, R. E.; Burant, J. C.; Dapprich, S.; Millam, J. M.; Daniels, A. D.; Kudin, K. N.; Strain, M. C.; Farkas, O.; Tomasi, J.; Barone, V.; Cossi, M.; Cammi, R.; Mennucci, B.; Pomelli, C.; Adamo, C.; Clifford, S.; Ochterski, J.; Petersson, G. A.; Ayala, P. Y.; Cui, Q.; Morokuma, K.; Malick, D. K.; Rabuck, A. D.; Raghavachari, K.; Foresman, J. B.; Cioslowski, J.; Ortiz, J. V.; Stefanov, B. B.; Liu, G.; Liashenko, A.; Piskorz, P.; Komaromi, I.; Gomperts, R.; Martin, R. L.; Fox, D. J.; Keith, T.; Al-Laham, M. A.; Peng, C. Y.; Nanayakkara, A.; Gonzalez, C.; Challacombe, M.; Gill, P. M. W.; Johnson, B. G.; Chen, W.; Wong, M. W.; Andres, J. L.; Head-Gordon, M.; Replogle, E. S.; Pople, J. A. *Gaussian 98*, revision A.7; Gaussian, Inc.: Pittsburgh, PA, 1998.

(60) Florián, J.; Warshel, A. *ChemSol*, version 2.1; University of Southern California: Los Angeles, CA, 1998.

(61) Sparks, T.; Hammock, B. Induction and regulation of juvenile hormone esterases during the last larval instar of the cabbage looper, *Trichoplusia Ni*. *J. Insect Physiol.* **1979**, *25*, 551–560.

(62) Abdel-Aal, Y. A. I.; Hammock, B. D. Transition state analogs as ligands for affinity purification of juvenile hormone esterase. *Science* **1986**, *233*, 1073–1075.

(63) Shiotsuki, T.; Huang, T. L.; Hammock, B. D. Affinity purification of mouse liver carboxylesterases with trifluoromethyl ketones as ligands. *J. Pestic. Sci.* **1994**, *19*, 321–324.

(64) Leo, A. J. Calculating log P_{oct} from structures. *Chem. Rev.* **1993**, *93*, 1281–1306.

(65) Thomas, T. C.; Székács, A.; Rojas, S.; Hammock, B. D.; Wilson, B. W.; et al. Characterization of neuropathy target esterase using trifluoromethyl ketones. *Biochem. Pharmacol.* **1987**, *40*, 2587–2596.

(66) Morgan, R. S.; McAdon, J. M. Predictor for sulfur–aromatic interactions in globular proteins. *Int. J. Pept. Protein Res.* **1980**, *15*, 177–180.

(67) Bencharit, S.; Morton, C. L.; Howard-Williams, E. L.; Danks, M. K.; Potter, P. M.; et al. Structural insights into CPT-11 activation by mammalian carboxylesterases. *Nat. Struct. Biol.* **2002**, *9*, 337–342.

(68) Thomas, B. A.; Church, W. B.; Lane, T. R.; Hammock, B. D. Homology model of juvenile hormone esterase from the crop pest, *Heliothis virescens*. *Proteins* **1999**, *34*, 184–196.

(69) Guthrie, J. P. Carbonyl addition reactions: Factors affecting the hydrate–hemiacetal and hemiacetal equilibrium constants. *Can. J. Chem.* **1975**, *53*, 898–906.

(70) Scott, W. J.; Zuman, P. Hydration–dehydration constants of α,α,α-trifluoroacetophenone by spectral and electrochemical methods. *J. Chem. Soc., Faraday Trans. 1* **1976**, 1192–1200.

(71) Abdel-Aal, Y. A. I.; Hammock, B. D. Apparent multiple catalytic sites involved in the ester hydrolysis of juvenile hormones by the hemolymph and by an affinity-purified esterase from *Manduca sexta* Johannson (Lepidoptera: Sphingidae). *Arch. Biochem. Biophys.* **1985**, *243*, 206–219.

(72) Olmstead, M. M.; Musker, W. K.; Hammock, B. D. Structure of the hydrate form of a β-thiotrifluoromethyl ketone, a potent esterase inhibitor. *Acta Crystallogr.* **1987**, *C43*, 1726–1728.

(73) Rablen, P. R.; Lockman, J. W.; Jorgensen, W. L. Ab initio study of hydrogen-bonded complexes of small organic molecules with water. *J. Phys. Chem. A* **1998**, *102*, 3782−3797.

(74) Johnstone, R. A. W.; Rose, M. E. A rapid, simple, and mild procedure for alkylation of phenols, alcohols, amides, and acids. *Tetrahedron* **1979**, *35*, 2169−2173.

(75) Drabowicz, J.; Mikolajczyk, M. An improved method for oxidation of sulfides to sulfoxides with hydrogen peroixde in methanol. *Synth. Commun.* **1981**, *11*, 1025−1030.

(76) March, J. *Advanced Organic Chemistry: Reactions, Mechanisms, and Structure*, 4th ed.; John Wiley & Sons: New York, 1992; p 1495.

(77) Ando, W.; Hanyu, Y.; Kumamoto, Y.; Takata, T. Synthesis of diisopropylidenethiirane (thiiranoradialene) and its reactions. *Tetrahedron* **1986**, *42*, 1989−1994.

(78) Moini, M.; Jones, B. L.; Rogers, R. M.; Jiang, L. F. Sodium trifluoroacetate as a tune/calibration compound for positive- and negative-ion electrospray ionization mass spectrometry in the mass range of 100−4000 Da. *J. Am. Soc. Mass Spectrom.* **1998**, *9*, 977−980.

(79) Dess, D. B.; Martin, J. C. Readily accessible 12-**I**-5 oxidant for the conversion of primary and secondary alcohols to aldehydes and ketones. *J. Org. Chem.* **1983**, *48*, 4155−4156.

(80) Ireland, R. E.; Liu, L. An improved procedure for the preparation of the Dess−Martin periodinane. *J. Org. Chem.* **1993**, *58*, 2899.

(81) Singh, R. P.; Cao, G.; Kirchmeier, R. L.; Shreeve, J. M. Cesium fluoride catalyzed trifluoromethylation of esters, aldehydes, and ketones with (trifluoromethyl)trimethylsilane. *J. Org. Chem.* **1999**, *64*, 2873−2876.

(82) Huang, T. L.; Villalobos, S. A.; Hammock, B. D. Effect of hepatotoxic doses of paracetamol and carbon tetrachloride on the serum and hepatic carboxylesterase activity in mice. *J. Pharm. Pharmacol.* **1993**, *45*, 458−465.

(83) Siegel, S. *Nonparametric statistics for the behavioral sciences*; McGraw-Hill Book Company: New York, 1956; p 312.